HHS Public Access

Author manuscript

Sci Transl Med. Author manuscript; available in PMC 2023 May 08.

Published in final edited form as:

Sci Transl Med. 2022 April 20; 14(641): eabm6586. doi:10.1126/scitranslmed.abm6586.

Reactive oxygen species–degradable polythioketal urethane foam dressings to promote porcine skin wound repair

Prarthana Patil[1], **Katherine A. Russo**[1], **Joshua T. McCune**[1], **Alonda C. Pollins**[2], **Matthew A. Cottam**[3], **Bryan R. Dollinger**[1], **Carlisle R. DeJulius**[1], **Mukesh K. Gupta**[1], **Richard D'Arcy**[1], **Juan M. Colazo**[1], **Fang Yu**[1], **Mariah G. Bezold**[1], **John R. Martin**[1], **Nancy L. Cardwell**[2], **Jeffrey M. Davidson**[4], **Callie M. Thompson**[5], **Adrian Barbul**[6,7], **Alyssa H. Hasty**[3,8], **Scott A. Guelcher**[1,9], **Craig L. Duvall**[1,*]

[1]Department of Biomedical Engineering, Vanderbilt University, Nashville, TN 37235, USA.

[2]Department of Plastic Surgery, Vanderbilt University Medical Center, Nashville, TN 37212, USA.

[3]Department of Molecular Physiology and Biophysics, Vanderbilt University School of Medicine, Nashville, TN 37232, USA.

[4]Department of Pathology, Microbiology and Immunology, Vanderbilt University School of Medicine, Nashville, TN 37232, USA.

[5]Vanderbilt Burn Center, Vanderbilt University Medical Center, Nashville, TN 37232, USA.

[6]Department of Surgery, Vanderbilt University Medical Center, Nashville, TN 37212, USA.

[7]Department of Surgery, Veterans Administration Medical Center, Nashville, TN 37212, USA.

[8]Veterans Affairs Tennessee Valley Healthcare System, Nashville, TN 37212, USA.

[9]Department of Chemical and Biomolecular Engineering, Vanderbilt University, Nashville, TN 37235, USA.

Abstract

Porous, resorbable biomaterials can serve as temporary scaffolds that support cell infiltration, tissue formation, and remodeling of nonhealing skin wounds. Synthetic biomaterials are less expensive to manufacture than biologic dressings and can achieve a broader range of

*Corresponding author. craig.duvall@vanderbilt.edu.

Author contributions: C.L.D. acquired funding and conceived and supervised the study. P.P. conceived and performed experiments, analyzed data, and wrote the manuscript. P.P., J.T.M., K.A.R., M.A.C., B.R.D., J.R.M., M.K.G., F.Y., M.G.B., and C.R.D. performed experiments. P.P., J.T.M., B.R.D., J.M.C., A.C.P., and N.L.C. performed in vivo experiments. P.P., R.D., J.T.M., and C.L.D. wrote the manuscript. J.M.D., S.A.G., A.H.H., A.B., and C.M.T. supervised the studies.

Competing interests: The authors confirm that there are no known conflicts of interest associated with this publication and that there has been no significant financial support for these efforts that could have influenced their outcome. C.L.D., P.P., J.R.M., M.K.G., R.D., J.T.M., and S.A.G. are the inventors on a published patent (10046086) and/or patent application (63/177,939) held/submitted by Vanderbilt University. These patents cover the PTK-UR compositions and methods of use.

SUPPLEMENTARY MATERIALS

www.science.org/doi/10.1126/scitranslmed.abm6586

Materials and Methods

Figs. S1 to S15

Tables S1 and S2

Data file S1

MDAR Reproducibility Checklist References (119–123)

physiochemical properties, but opportunities remain to tailor these materials for ideal host immune and regenerative responses. Polyesters are a well-established class of synthetic biomaterials; however, acidic degradation products released by their hydrolysis can cause poorly controlled autocatalytic degradation. Here, we systemically explored reactive oxygen species (ROS)–degradable polythioketal (PTK) urethane (UR) foams with varied hydrophilicity for skin wound healing. The most hydrophilic PTK-UR variant, with seven ethylene glycol (EG7) repeats flanking each side of a thioketal bond, exhibited the highest ROS reactivity and promoted optimal tissue infiltration, extracellular matrix (ECM) deposition, and reepithelialization in porcine skin wounds. EG7 induced lower foreign body response, greater recruitment of regenerative immune cell populations, and resolution of type 1 inflammation compared to more hydrophobic PTK-UR scaffolds. Porcine wounds treated with EG7 PTK-UR foams had greater ECM production, vascularization, and resolution of proinflammatory immune cells compared to polyester UR foam–based NovoSorb Biodegradable Temporizing Matrix (BTM)–treated wounds and greater early vascular perfusion and similar wound resurfacing relative to clinical gold standard Integra Bilayer Wound Matrix (BWM). In a porcine ischemic flap excisional wound model, EG7 PTK-UR treatment led to higher wound healing scores driven by lower inflammation and higher reepithelialization compared to NovoSorb BTM. PTK-UR foams warrant further investigation as synthetic biomaterials for wound healing applications.

One-sentence summary:

Hydrophilic polythioketal urethane foam scaffolds promote skin wound healing in pigs.

Designing degradable dressings

Synthetic scaffolds are an attractive option for dressings to treat skin wounds because they are shelf stable, have tunable and defined chemical compositions, and are more affordable than naturally derived scaffolds or cell-based dermal substitutes. Here, Patil and colleagues investigated the role of scaffold hydrophilicity in polythioketal-based polyurethane (PTK-UR) foam scaffold resorption and promotion of tissue regeneration in wound healing. They found that hydrophilic scaffolds with seven ethylene glycol units between the thioketal bonds in the polymer backbone exhibited optimal reactive oxygen species–dependent degradation and porcine skin wound healing, including ischemic flap excisional wounds. Results support further investigation of PTK-UR formulations as alternatives to commercially available wound matrices.

INTRODUCTION

Chronic wounds affect about 4.5 million people in the United States, resulting in considerable economic burden of $96.8 billion per year (1, 2). Diabetes, obesity, and vascular diseases predispose patients to delayed or incomplete skin wound closure that can lead to lower limb amputation (1, 3, 4) and high recurrence and mortality rates (5, 6). Nonhealing wounds have persistent, low-grade inflammation with an influx of polymorphic mononuclear leukocytes that secrete inflammatory cytokines, proteolytic enzymes, and reactive oxygen species (ROS) (7). Nonhealing wounds driven by vascular insufficiencies are often compounded by ischemia-r eperfusion injury, which triggers ROS generation and tissue damage (8), whereas bacterial infection can further exacerbate the local inflammatory

imbalance (10). Excess ROS causes oxidative stress, which diminishes critical wound healing processes such as angiogenesis, extracellular matrix (ECM) deposition, and the healing capacity of fibroblasts and keratinocytes (9).

The standard of care for treating chronic wounds includes tissue debridement, moisture control, and use of advanced wound dressings with or without active compounds to reduce infection (11). Wound dressing biomaterials comprise either naturally derived or synthetic polymers that act as a provisional matrix, providing mechanical support and promoting cellular infiltration, neovascularization, ECM deposition, and consequently accelerated defect repair (12). Acellular wound dressings based on animal-derived ECM components are well established. The first of its kind, Integra Bilayer Wound Matrix (BWM), designed by Yannas *et al.* (13), has a long clinical track record; in diabetic foot ulcers, Integra BWM achieves full closure in 51% of wounds by 16 weeks, compared to 32% by standard wound care (14). Similarly, OASIS ULTRA wound dressings manufactured from porcine small intestinal submucosa decrease the time required for complete wound closure and lower the reoccurrence of venous ulcers (15). ECM-based dressings have been adopted for clinical use (16), but they are challenged by raw material sourcing, reproducible processing techniques, cross-species immunogenicity risk, and exuberant costs (17).

Fully synthetic dermal materials provide reproducible and cost-effective product fabrication while also affording controlled tuning of chemical composition, microarchitecture, physiochemical properties, and degradation profiles (18–20). Hydrolytically degradable polyesters (PEs) are the main class of synthetic polymers that have so far been applied clinically as resorbable wound dressings (21), with Restrata and NovoSorb Biodegradable Temporizing Matrix (BTM) being two examples. Restrata is an electrospun poly(lactic acid-glycolic acid) (PLGA) (10:90) and polydioxanone mat, whereas NovoSorb is a polyurethane (PU) foam made from ethyl lysine diisocyanate, lactic acid/ethylene glycol (EG) chain extender, and polycaprolactone polyol with a removable PU overlayer (22, 23). Both products have gained broad U.S. Food and Drug Administration approval for indications spanning traumatic and postsurgical wounds, second-degree burns, pressure ulcers, and diabetic ulcers.

Highly porous PU foams, such as NovoSorb, offer interconnected pores that allow for efficient cell infiltration and low material mass, which reduces production costs and the quantity of potentially inflammatory or cytotoxic degradation products (24). PU materials are also tunable, through variation of either the polyol or isocyanate- containing component. Isocyanates have been paired with aliphatic PE such as poly(lactic acid) (25), PLGA, polycaprolactone (26), and their blends for many tissue engineering applications (27–30). However, degradation of PE-based materials releases acidic by-products that can activate an uncontrolled autocatalytic degradation mechanism (31) and trigger inflammation (32).

Hydrolytically stable, polymeric biomaterials that are degraded by cell-generated stimuli are a promising alternative to PE-based materials (33). We previously innovated a class of polythioketal (PTK)–based PU scaffolds that provided more temporally controlled degradation kinetics compared to PE materials in rat wounds and promoted robust tissue integration both in rat and porcine skin wounds (34, 35). We have also shown that PTK–

cross-linked polyethylene glycol (PEG)–maleimide hydrogels promote tissue infiltration and neovascularization in mice, confirming the biocompatibility of hydrophilic PTK-based materials in physiologically relevant environments (36).

Here, we posited that scaffold hydrophilicity is an important parameter for optimization of wound healing performance of PTK urethane (PTK-UR) dermal substitutes. This hypothesis was motivated by previous studies showing that integration of highly hydrophilic polymers such as PEG or zwitterions into tissue engineering materials can increase scaffold degradation (37), increase tissue infiltration (25) into hydrolytically-degradable PE-URs, and trigger regenerative immunophenotypes while decreasing fibrosis (38). Toward this end, we generated a library of ROS-responsive PTK-UR foams with controlled variation of the PTK diol component to contain different lengths of EG units between the thioketal (TK) bonds in the polymer backbone. We hypothesized that increased hydrophilicity of PTK-UR scaffolds would increase TK group reactivity with water- soluble ROS, thus improving scaffold ROS scavenging and ultimately promoting a faster and more favorable rate of material resorption in vivo. The primary goals of these studies were to establish the functional importance of PTK-UR scaffold hydrophilicity on wound healing and to benchmark leading PTK-UR formulations against current standards of care in clinically relevant porcine skin wound repair models that recapitulate full-thickness and ischemic skin wounds.

RESULTS

Synthesis and characterization of PTK diol

To vary polyol hydrophilicity, we incorporated increasing units of EG between TK bonds in the PTK diol backbone using three different dithiol monomers with zero (EG0), one (EG1), or two (EG2) EG repeats. Using previously reported polymerization techniques (34, 35, 39, 40), we synthesized EG0, EG1, and EG2 PTK dithiols through condensation polymerization of butanedithiol, mercaptoethyl ether, and 2,2′-(ethylenedioxy) diethanethiol monomers, respectively (Fig. 1A and fig. S1). Purified dithiol polymers were functionalized with 2-bromoethanol to obtain EG0, EG1, and EG2 PTK diols. The formation of TK bonds was confirmed through ^{1}H nuclear magnetic resonance (NMR); δ at 1.6 parts per million (fig. S1). Dithiol monomers containing an EG content greater than 2 did not efficiently polymerize with this condensation reaction, resulting in poor conversion, likely forming cyclic structures from individual monomers rather than linear chains of multiple monomers.

To address the drawbacks of this approach and to further increase the EG content, we developed an alternative polymerization strategy based on the polyaddition reaction of amine-reactive heterobifunctional PEG and a small TK diamine cross-linker/monomer. The TK diamine was synthesized from a protected cysteamine derivative and dimethoxy propane as confirmed by ^{1}H NMR spectroscopy (fig. S2) (41). To obtain a PTK diol with seven EG repeats between TK groups in the polymer backbone (EG7 PTK diol), monofunctional PEG400 nitrophenylcarbonate (HO-PEG-NPC) was first synthesized through the reaction of 400 gmol^{-1} PEG diol (PEG400) with *p*-nitrophenyl chloroformate at a stoichiometric ratio of 1:1, yielding a mixture of primarily OH-PEG-NPC and a small percentage of homobifunctional PEG400 dinitrophenylcarbonate (NPC-PEG-NPC) macromers. The bifunctional PEG macromers functioned as “chain extenders” through reaction with multiple

TK diamines (fig. S2). Gel permeation chromatography analysis revealed that all PTK diol polymer chains had relatively low dispersity (Đ < 1.2) and a number-average molecular weight (M_n) between 1500 and 2200 $gmol^{-1}$ (fig. S3A). The resulting EG0, EG1, EG2, and EG7 PTK diols were composed respectively of 11.7, 10.2, 8.2, and 2 TK units per polymer chain (fig. S3C), and the presence of terminal hydroxyl functional (OH) groups was verified by their characteristic Fourier transform infrared absorbance peak at 3400 cm^{-1}. Hydroxyl functionalization was quantified indirectly through ^{19}F NMR upon reaction with 4-fluorophenyl isocyanate. Experimentally determined hydroxyl numbers closely matched theoretical values, indicating successful hydroxyl functionalization (~85%) and the presence of terminal OH groups for isocyanate reactivity in subsequent foaming reactions (fig. S3C).

PTK-UR scaffold hydrophilicities positively correlate with EG content and log *P* values

To create a PU foam with interconnected porous structure, the terminal OH groups on PTK diols or PE trimeric polyols (trimer t, 60% ε-caprolactone, 30% glycolide, and 10% d,l-lactide composition) were reacted with isocyanate groups present on a lysine triisocyanate (LTI) cross-linker in the presence of TEGOAMIN33 as a catalyst and water as a blowing agent (Fig. 1B). LTI was used on the basis of our previous porcine ischemic wound healing studies, which showed favorable response to PTK-UR scaffolds made with LTI as compared to scaffolds formulated using a nondegradable isocyanate component (35). Two PE-based triols with molecular weights of 900 $gmol^{-1}$ (900t PE) and 1500 $gmol^{-1}$ (1500t PE) were used to fabricate PE-UR scaffold controls. Formulation specifications for each foam are provided in table S1. PTK-UR scaffolds with similar porosity (86.8 to 91.5%) and comparable pore sizes (74.2 to 133.3 μm) were fabricated from the respective EG0, EG1, EG2, and EG7 PTK diols. Efficient covalent cross-linking between OH and NCO groups of LTI was confirmed on the basis of the low soluble fractions (sol fractions) for each scaffold (fig. S4).

Contact angle measurements on PU films were performed to experimentally gauge scaffold hydrophilicity; EG7 PTKUR demonstrated the lowest contact angle (52.7° ± 5.8°) compared to EG0 (79.2° ± 3.3°), EG1 (66.5° ± 2.9°), and EG2 (61.2° ± 2.3°) (Fig. 1C). The measured contact angles positively correlated with the theoretical partition coefficients (log *P*) of PTK diols (Fig. 1D). Determination of the swelling ratio for the PTKUR materials (fig. S4) also supported that our EG series yielded a set of PTKUR scaffolds with controlled variation of relative hydrophilicity. Mechanical properties (compressive modulus determined under hydrated conditions) of the scaffolds were all similar, with EG0, EG1, EG2, and EG7 PTK-UR scaffolds showing moduli of 75.0 ± 7.8, 61.4 ± 6.6, 78.5 ± 12.3, and 67.1 ± 10.7 kPa, respectively (Fig. 1E); these properties are a good approximation of the reported tensile modulus of human skin (60 to 850 kPa) (42, 43). Although the wet modulus of all PTK-UR formulations did not significantly differ, the modulus of the 900t ($P < 0.05$ versus all PTK-UR formulations) and 1500t PE-UR (1500t versus EG0 and 1500t versus EG2, $P < 0.01$) scaffolds showed a small but significant decrease compared to the PTK-URs. These data collectively indicate that the PTK-UR scaffold formulations have similar mechanical and structural properties, allowing for controlled study of the biological effects of relative scaffold hydrophilicity.

Increased PTK-UR scaffold hydrophilicity improves ROS reactivity

TK bonds are broken through irreversible reaction with ROS such as hydroxyl radicals (•OH), superoxide (O_2^-), hydrogen peroxide (H_2O_2), and hypochlorite (ClO^-) (34, 40, 44). This provides an opportunity to create TK-based biomaterials whose ROS-dependent degradation mechanism also provides antioxidant function. Using 1,1-diphenyl-2-picrylhydrazyl (DPPH) as a model free radical, the antioxidant activity of PTK-UR scaffolds was significantly higher than that of PE-UR scaffolds ($P < 0.0001$ at 3, 6, 12, 24, 30, and 36 hours; Fig. 1F). The predominantly organic solvent mixture used to perform the DPPH assay (80:20 ethanol:H_2O) does not accurately reflect in vivo conditions, and experimental results may not reflect the differences in TK bond accessibility that occur in a fully aqueous system. Despite these conditions, EG1, EG2, and EG7 PTK-UR formulations showed significantly ($P < 0.001$) higher radical scavenging compared to EG0 PTK (at 6, 12, and 24 hours) in this polar solvent mixture (Fig. 1F). To evaluate the effect of PTK composition on antioxidant function and cytoprotection in aqueous environments more directly, we exposed NIH 3T3 murine fibroblasts to varying concentrations of H_2O_2 (25 and 50 μM) in the presence of the series of PTK diols (normalized TK molar content). All PTK diol treatments offered significant ($P < 0.05$) protection from H_2O_2 (25 μM)–mediated cell toxicity compared to 900t PE treatments. At the higher concentration of H_2O_2 (50 μM), EG7 PTK formulation rescued cell viability to a significantly ($P < 0.0001$) higher degree than all other treatment groups, offering nearly twofold greater viability than the next most hydrophilic PTK (EG2 PTK) (Fig. 1G). These data highlight an important cytoprotective benefit of ROS scavenging in the PTK diols and the correlation of PTK radical reactivity with hydrophilicity. To further evaluate the antioxidant activity of EG7 PTK-UR scaffolds, we implanted 900t PE-UR and EG7 PTK-UR foams in the subcutaneous space of C57BL6 mice. Scaffolds explanted 4 days after implant showed that the EG7 PTK-UR foams had significantly ($P < 0.01$) lower ROS concentrations than 900t PE-UR scaffolds measured by Amplex Red (a H_2O_2 probe) (Fig. 1H). These data suggest that the presence of accessible TKs in more hydrophilic PU scaffolds provides antioxidant activity.

To investigate ROS-dependent degradation kinetics of PTK-UR and PE-UR scaffolds, we incubated PU samples in phosphate-buffered saline (PBS) or increasing concentrations of oxidative media (Fig. 1I). PTK-UR scaffolds incubated in hydrolytic media (PBS) remained intact with minimal mass loss over the course of the experiment. There was a small but significant ($P < 0.05$) mass loss of EG7 PTK-UR scaffolds in PBS at days 14, 20, and 30 due to the mechanics of manipulating the significantly ($P < 0.0001$) more swollen EG7 PTK-UR scaffolds (fig. S4A). However, unlike 900t and 1500t PE-UR scaffolds, all four PTK-UR foam compositions degraded in oxidative media (0.2 and 2% H_2O_2) simulated by •OH from the Fenton reaction between H_2O_2 and catalytic amounts of $CoCl_2$. The PTK-UR scaffold mass loss was ROS concentration dependent for all compositions. There were no significant differences in the rate of degradation between the different PTK-UR scaffold formulations at the highest hydroxyl radical concentrations at days 14, 20 and 30. However, at lower concentrations (0.2 and 2% H_2O_2), significantly ($P < 0.01$) higher mass loss in EG7 PTK-UR scaffolds was recorded compared to EG0, EG1, and EG2 PTK-UR formulations, despite the EG7 PTK diol having the lowest TK bond backbone density contributing to oxidative degradation. Modeling analysis showed that the EG7 PTK-UR scaffolds had a

higher degradation rate constant than all the PTK-UR formations at 0.2 and 2% ROS concentrations and that, under mild ROS conditions (0.2% H_2O_2), the rate of degradation increased with an increase in EG content (Fig. 1J). Morphological changes such as loss in porous architecture and qualitative increase in pore size were observed in scanning electron microscopy images of PTK-UR scaffolds incubated in oxidative media (Fig. 1K and figs. S5 and S6). No apparent changes were visible in PBS-incubated samples, suggesting hydrolytic stability. Together with the DPPH and cytoprotection assays, these data demonstrate that TK groups in the more hydrophilic (higher EG content) scaffolds are more accessible for ROS scavenging.

Effects of scaffold chemistry on porcine excisional wound healing

To investigate the tissue response to synthetic PU scaffolds, we implanted 900t PE-UR and PTK-UR scaffolds in rectangular 2 cm– by–1 cm full-thickness skin wounds on the dorsal region of Yorkshire pigs. Ten days after scaffold implantation, we observed varying degrees of scaffold integration within the wound bed (Fig. 2A, top row). An increase in tissue integration and homogeneity of distribution throughout the wound bed was observed for the wounds treated with EG7 PTK-UR compared to all other treatments (Fig. 2, A and B). Tissue infiltration within the pores of the scaffolds also positively correlated ($R^2 = 0.92$) with EG content in the PTK diol used to fabricate the scaffolds (Fig. 2C and fig. S8A). The highest tissue infiltration was seen in EG7 PTK treatments (77 ± 3%) compared to the more hydrophobic PTK chemistries. Vascular density, visualized through immunohistochemistry (IHC) for von Willebrand factor (vWF), also positively correlated with EG content (Fig. 2, A and D, and fig. S8B) and thus overall scaffold hydrophilicity.

Scaffold hydrophilicity affects inflammatory cellular infiltrates and wound microenvironment

Inflammatory responses to implanted biomaterials can dictate the quality of tissue repair in skin wounds (45–47). We investigated spatial distribution of inflammatory cell infiltrates within implanted PU scaffolds 10 days after implantation. All five PU treatments recruited inflammatory cells, including myeloperoxidase-positive (MPO^+) neutrophils and $CD206^+$ macrophages, into the scaffolds (Fig. 2E). Active recruitment of neutrophils from the bloodstream to implanted biomaterials can propagate inflammation through secretion of proinflammatory cytokines, interleukins (ILs), and ROS (48, 49). MPO staining was localized around scaffold remnants, suggesting recruitment of neutrophils to the scaffold-tissue interface. EG7 PTK scaffolds were associated with significantly ($P < 0.05$) fewer neutrophils (Fig. 2F) compared to all other treatments. A complementary immunohistochemical analysis for 8-hydroxy-2′-deoxyguanosine (8-OhdG), a marker for free radical–induced oxidative stress (50), showed significantly lower staining in EG7 PTK-UR–treated wounds compared to PE-based 900t PE-UR treatments (fig. S9). Macrophage polarization can also play an important role in biomaterial integration and wound healing (45, 51, 52). We investigated the polarization of M2 macrophages within implanted PU foams and saw a significant ($P < 0.05$) increase in $CD206^+$ macrophages in EG7 PTK–treated wounds compared to 900t PE treatment (Fig. 2, E and G). To complement histological analysis of wound tissue, we performed bulk tissue gene analysis of inflammation- associated transcripts; EG7 PTK-UR scaffold–treated

wounds were associated with consistently decreased expression of inflammation- related mRNAs including colony-stimulating factors (*CSF2* and *CSF3*), tumor necrosis factor–α (*TNFA*), interleukin-1β (*IL1B*), interleukin-12A (*IL12A*), inflammatory chemokine ligand 8 (*CXCL8*), and nitric oxide synthase 2 (*NOS2*) compared to all other treatment groups (Fig. 2H).

EG7 PTK-UR scaffolds promote wound closure, reepithelialization, and tissue repair in pigs

Next, we investigated wound closure rates of PU foam–treated pig skin wounds over an extended time course (24 days). Wound area for all scaffold treatments decreased over a period of 24 days (Fig. 3A and fig. S10A). Twenty-four days after surgery, EG7 PTK–treated wounds achieved 70.5% closure compared to only 52.9 and 53.8% closure observed in EG1 and EG2 PTK treatments, as well as 49.2% for 900t PE (Fig. 3C). All EG0 PTK-UR scaffolds were extruded from the wounds 20 to 22 days after implantation, resulting in spontaneous wound contraction (fig. S10A). We observed poor EG0 scaffold integration with skin wounds despite initially similar percentage of tissue infiltration between EG0 and EG1 scaffold pores (figs. S8A and S10B), emphasizing the importance of scaffold hydrophilicity in biomaterial-tissue integration. Because of the premature extrusion and loss of EG0 scaffolds, this treatment group was not included in subsequent analyses.

Complete wound closure is associated with migration of epidermal cells from the surrounding wound margins toward the center, fully covering the granulation tissue with new epithelium (53). We, therefore, sought to evaluate epidermal layer reestablishment of PU-treated excisional pig wounds through visualization of keratin14^{+} basal keratinocytes. Cytokeratin14 IHC revealed that at day 24, 90% of EG7 PTK-UR–treated wounds had completely epithelialized, with 99.2% of the wound covered with a thin, uniform neo-epidermal layer (Fig. 3, B and C). In contrast, none of the other PU treatments resulted in complete reepithelialization of the wounds, with an average of 49.6, 55.0, and 61.0% wound closure observed in 900t PE, EG1, and EG2 PTK treatments, respectively (Fig. 3C). In addition to incomplete epithelialization of wounds with these treatments, excessive epidermal thickening suggests an immaturity of the reepithelialization process due to persistent inflammation and presence of hyperproliferative keratinocytes with minimal migration (7, 54, 55).

Histological analysis of the skin wounds at the day 24 end point revealed tissue integration and scaffold resorption across all four PU treatments (Fig. 3D, low magnification). EG1 PTK and EG2 PTK scaffold remnants were primarily present in the lower portion of the granulation tissue, surrounded by a dense halo of immune cells. On the contrary, EG7 PTK-UR scaffolds were uniformly distributed within the granulation tissue and were not associated with dense pockets of inflammatory cells (Fig. 3D, high magnification). To further investigate the effects of scaffold chemistry on different aspects of skin repair and restoration, trichrome and hematoxylin and eosin (H&E) sections were semiquantitatively assessed by a treatment-blinded histopathologist (scoring rubric shown in table S2). Scoring of the wounds indicated that EG7 PTK-UR–treated wounds had higher- quality granulation tissue (Fig. 3E), more extensive ECM deposition, and reconstruction of dermal architecture

(Fig. 3F) compared to wounds treated with 900t PE. There was also an overall increase in quality and quantity of granulation tissue and collagen deposition associated with higher EG content, as indicated by granulation and collagen scores across the EG series. We also observed significantly ($P < 0.01$) higher epithelialization of EG7 PTK–treated wounds compared to all other PU treatments (Fig. 3G). EG7 PTK– treated wounds were associated with lower inflammatory infiltrate, including mononuclear cells and foreign body giant cells (FBGCs), compared to 900t PE (Fig. 3H). The cumulative wound score revealed significantly ($P < 0.01$) improved quality of wound healing and repair of EG7 PTK–treated wounds compared to more hydrophobic PE, EG1, and EG2 PTK formulations (11.5 ± 1.34, 5.5 ± 2.5, 6.9 ± 2.7, and 7.33 ± 2.1, respectively; Fig. 3I).

Modulation of innate and adaptive immune response by EG7 PTK-UR scaffolds in pig skin wounds

Inflammatory response to scaffold chemistry involving both innate and adaptive immune cells can affect biomaterial-tissue integration and wound repair (49, 56–58). We hypothesized that increased hydrophilicity of PU scaffolds contributes to decreased proinflammatory microenvironment within the wound, ultimately decreasing biomaterial-associated fibrosis. Accordingly, we evaluated the effects of scaffold chemistry on the recruitment of immune cells at the scaffold-tissue interface. Twenty-four days after PU scaffold implantation, we confirmed the presence of both innate ($CCR7^+$ M1 macrophages) and adaptive ($CD3^+$ T cells) immune cells within the tissue margins of all implanted scaffold formulations (Fig. 4A). CCR7 IHC revealed a dense association of M1 macrophages with scaffold remnants, and CCR7 staining intensity decreased as a function of distance from the scaffold edge. There was also significantly ($P < 0.05$) lower staining intensity surrounding EG7 PTK scaffold remnants compared to 900t PE, EG1, and EG2 PTK scaffolds at distances greater than 50 μm from scaffold edge (Fig. 4B). Unlike EG7 PTK scaffolds, the other treatment groups were associated with a dense layer of M1-polarized macrophages and FBGCs surrounding scaffold remnants within the wound bed, suggesting a persistent inflammatory response to the scaffold and/or its degradation products. To evaluate the adaptive immune response, we also quantified the density of CD3-positive T cells surrounding scaffold pieces at day 24, finding significantly ($P < 0.001$) lower density surrounding EG7 PTK scaffold remnants compared to EG1 and EG2 PTK scaffolds (Fig. 4C). T cells are known to produce IL-6, IL-12, and IL-17 proinflammatory molecules in response to synthetic biomaterial implants, propagating inflammation, and fibrosis (59, 60). In addition to immune cells, we also looked for the presence of alpha smooth muscle actin (aSMA) expression in myofibroblasts surrounding scaffolds. We observed organization of αSMA^+ myofibroblasts surrounding EG1 PTK and EG2 PTK scaffold fragments but not EG7 PTK scaffolds (Fig. 4A). The concentric spatial organization of M1 macrophages, myofibroblasts, and T cells suggests an active foreign body response against the more hydrophobic PTK-UR scaffold chemistries, similar to the response elicited by nondegradable implants (46, 61). These results suggest that the higher ROS degradability and scavenging potential of the more hydrophilic PTK-UR scaffolds are a critical factor in reducing the foreign body response to the biomaterials. It is also possible that the types of proteins that adsorb preferentially to hydrophilic versus hydrophobic material surfaces play a role in downstream macrophage polarization (62–64) and ultimate healing response.

To further evaluate the inflammatory microenvironment within PU scaffold–treated wounds, we quantified bulk tissue expression of proinflammatory genes (Fig. 4D). We observed significantly ($P < 0.05$) lower expression of *TNFA*, a proinflammatory cytokine, in EG7 PTK–treated wounds compared to EG1 and EG2 PTK treatments. Lower expression was also seen for proinflammatory mediators *IFNG* and *CSF2*.

Because of the limited availability of porcine-specific antibodies for IHC, we used a mouse subcutaneous model to further characterize the immune cell populations and pheno types that infiltrate the scaffolds. This flow cytometry study (gating strategies outlined in fig. S11) focused on EG2 versus EG7 PTK-UR scaffolds, because these materials both effectively integrate in vivo while still showing significantly different hydrophilicity-driven biological responses. Scaffolds were implanted into ventral subcutaneous pockets in C57BL6 mice, and scaffold-infiltrating cells were analyzed at 1, 2, and 3 weeks after implantation. After 1 week, we observed similar proportions of $CD45^+$ leukocytes, $CD11b^+CD11c^-F4/80^+$ macrophages (20% of all leukocytes), $CD11b^+F4/80^-$ monocytes/neutrophils (~40% of all leukocytes), and $CD11c^+F4/80^-$ dendritic cells (DCs) (~15% of all leukocytes) within the EG2 and EG7 scaffolds (fig. S12). Over a period of 3 weeks, infiltrating leukocyte populations significantly ($P < 0.01$) decreased in EG7 PTK scaffolds but remained constant in EG2 PTK scaffolds, suggesting an unresolved inflammatory response. We observed a significant ($P < 0.01$) decrease in $CD11b^+CD11c^-F4/80^+$ macrophage population in EG7 PTK scaffolds compared to EG2 scaffolds. Decreases in $CD11b^+F480^-$ monocyte and neutrophil populations were also observed. After 3 weeks of scaffold implantation, we observed significantly ($P < 0.001$) lower numbers of myeloid populations including $CD11b^+F4/80^-$ monocytes and neutrophils, $CD11b^+CD11c^-F4/80^+$ macrophages, and $CD11c^+F4/80^-$ DCs, as well as lymphoid-derived $\alpha\beta^+$ T cells, $CD4^+$ T helper (T_H) cells, and $CD8^+$ cytotoxic T lymphocytes present in EG7 PTK cellular infiltrates compared to EG2 PTK (Fig. 4E). On further analysis of T cell phenotypes, we saw a significantly higher percentage of $CD4^+FoxP3^+$ regulatory T cells ($P < 0.001$) and $CD4^+GATA3^+$ T_H2 cells ($P < 0.01$) within EG7 PTK scaffolds compared to EG2 PTK-UR scaffolds (Fig. 4F). We also detected a higher number of $\gamma\delta$ T ($P < 0.001$) cells associated with EG7 PTK scaffolds; these cells are a source of fibroblast growth factor 9 (FGF9) and kerat inocyte growth factor, which are both known to support reepithelialization and hair follicle neogenesis after wounding (65, 66). We observed significantly ($P < 0.05$) higher expression of CD301b, a macrophage galactose-type C-type lectin 2 (Mgl2) on $CD206^+$ macrophages isolated from EG7 PTK compared to EG2 PTK scaffolds (Fig. 4G). $CD206^+CD301b^+$ macrophage subtypes support effective skin repair through the production of platelet-derived growth factors (PDGFs), transforming growth factor beta (TGFβ), and insulin-like growth factor (IGF), resulting in fibroblast proliferation, migration, and collagen accumulation (67–69).

EG7 PTK-UR dermal substitute triggers pro-healing gene expression

In addition to analysis of immune response, we measured the effects of scaffold chemistry on the expression of genes related to granulation tissue formation, proliferation, and remodeling processes of wound healing in day 24 pig wounds (Fig. 5). We observed that EG7 PTK scaffold–treated wounds had about fourfold higher expression of genes encoding ECM proteins that comprise granulation tissue, including collagen I, III, V, and

XIV (*COL1A2*, *COL3A1*, *COL5A2*, and *COL14A1*) and tenascin (*TNC*). Integrins such as integrin β_1 (*ITGB1*) ($P < 0.05$), integrin β_3 (*ITGB3*) ($P < 0.05$), and integrin α_v (*ITGAV*) ($P < 0.05$), known to play important roles in cell adhesion, migration, and proliferation (70, 71), were also significantly up- regulated in EG7 PTK treatments. Transforming growth factor–β (*TGF*-β) pathway–related genes such as *SMAD3* ($P < 0.05$) and *TGFB3* ($P < 0.05$), known to promote collagen biogenesis and polarization of macrophages to M2 prohealing phenotype (72), were also significantly up-regulated in EG7 PTK–treated wounds compared to other treatments. Matrix metalloproteinases (*MMP2/7/9*), which are known to play important roles in collagen remodeling and recruitment of endothelial cells for neovascularization (73, 74), were significantly ($P < 0.05$) up-regulated in response to EG7 PTK treatments with respect to other PE and PTK treatments. EG7 samples expressed lower amounts of *MMP1*, a type 1 collagenase up-regulated in chronic wounds (75), relative to EG1 and EG2 PTK treatments. We also observed an increase in *TIMP2* (tissue inhibitor of metalloproteinase), an important inhibitor of MMPs produced by basal keratinocytes, in EG7 PTK–treated wounds. Combined with the MMP expression data, this suggests that a homeostatic balance between MMPs and their inhibitors was achieved, reflective of active remodeling of wounds in a more mature stage of healing for the EG7-treated group (76). Similar trends of increased gene expression were observed in EG7 samples for genes such as insulin-like growth factor (*IGF*), fibroblast growth factor 7 (*FGF7*), connective tissue growth factor (*CTGF*), and platelet-derived growth factor (*PDGF*), soluble mediators that promote cell proliferation and migration to drive skin wound granulation, vascularization, and reepithelialization (77).

Benchmarking EG7 PTK-UR against clinically approved dermal substitutes

Performance of the EG7 PTK-UR scaffolds was tested in pig skin wounds in comparison to clinically approved dermal substitutes: collagen- and proteoglycan-based Integra BWM (Integra Life Sciences) and PE-UR NovoSorb BTM (PolyNovo). We implanted porcine full-thickness skin wounds with EG7 PTK, NovoSorb, or Integra and measured wound closure over time as well as histological outcomes at 31 days after implantation. All three dermal substitutes facilitated tissue infiltration and wound closure over a period of 31 days (Fig. 6A and fig. S13A). Integra provided significantly less wound stenting than EG7 PTK scaffolds for the first 10 days, whereas the commercial foam NovoSorb and EG7 PTK performed similarly in this metric. In later stages, EG7 PTK–treated wounds resolved at a similar rate to Integra with no significant differences in the rate of wound closure. However, we observed significantly ($P < 0.05$) increased rates of wound closure in EG7 PTK and Integra versus NovoSorb at days 14, 17, 19, and 21 after implantation. Upon removal of the nondegradable PU layer (performed according to the manufacturer's guidelines), the wound area of NovoSorb-treated wounds significantly decreased ($P < 0.05$), suggesting rapid loss of stenting provided by the protective layer, followed by consequent wound contraction (Fig. 6B). In addition to wound closure, we measured vascular perfusion of scaffold-treated wounds using laser Doppler perfusion imaging (LDPI) (fig. S13B). EG7 PTK-UR– treated wounds were significantly ($P < 0.0001$) more perfused than those treated with Integra and NovoSorb at earlier time points (days 10 and 17), suggesting higher neovascularization (Fig. 6C). Removal of the temporary epidermal layer equivalent membranes from Integra and NovoSorb (Fig. 6B, indicated by arrows) resulted in disruption of granulation tissue, causing

re-wounding and increased perfusion within the wounds at days 17 and 24, respectively (fig. S13B).

In all three treatment groups, histological examination of scaffold-treated wounds revealed formation of granulation tissue along with the reestablishment of an epidermal layer. Trichrome- and H&E-stained sections revealed dense cellularity around NovoSorb scaffold remnants along with the formation of FBGCs that were minimally present in EG7 PTK–treated wounds (Fig. 6D). EG7 PTK-UR–treated wounds were composed of denser, more organized collagen deposition, along with decreased cellularity around scaffold remnants. These observations indicate that the EG7 PTK-UR–treated wounds were more mature and had transitioned into a more advanced remodeling phase relative to NovoSorb-treated wounds. Treatment- blinded histopathological scoring of these sections revealed similar collagen deposition, reepithelialization, and FBGC density between Integra- and EG7 PTK– treated wounds (Fig. 6E). In contrast, NovoSorb-treated skin wounds showed significantly ($P < 0.01$) lower collagen deposition with loosely arranged fibers, incomplete reepithelialization, more persistent inflammatory infiltrate, and formation of FBGCs. Cumulative wound healing scores revealed significantly ($P < 0.0001$) decreased quality of wound healing of NovoSorb-treated wounds compared to Integra and EG7 PTK-UR treatments, with no significant differences detected between the latter two materials. The collective EG7 PTK-UR histology from all time points was also aggregated and analyzed for in vivo scaffold degradation, showing that EG7 PTK-UR scaffolds underwent relatively constant resorption over time that was still ongoing 31 days after implantation (fig. S14).

Effective dermal repair and immune modulation by EG7 PTK-UR treatments compared to NovoSorb

Next, we thoroughly characterized the microenvironment of EG7 PTK-UR scaffold–treated pig wounds versus the more structurally analogous, synthetic NovoSorb PU foam–treated wounds. To complement the LDPI data, we measured vasculature within scaffold-treated wounds using vWF IHC and observed significantly ($P < 0.0001$) higher blood vessel density within EG7 PTK–treated wounds compared to those treated with NovoSorb (Fig. 7, A and B). To further examine the differences in dermal repair and remodeling between the two foam dermal substitutes, we analyzed expression of genes involved in ECM deposition and remodeling along with growth factors implicated in dermal wound healing. Transcriptional analysis revealed significantly ($P < 0.05$) higher expression of *COL1A2*, *COL3A1*, *COL5A2*, *COL14A1*, and *TNC* in EG7 PTK–treated wounds compared to NovoSorb- treated wounds (Fig. 7C). In addition, significantly ($P < 0.05$) higher expression of ECM remodeling enzymes including cathepsin K (*CTSK*), *MMP2*, *MMP7*, and *TIMP2* was seen in EG7 PTK–treated wounds compared to NovoSorb-treated wounds. Factors involved in collagen biosynthesis and ECM remodeling such as *TGFB3* and *SMAD3* were also significantly ($P < 0.05$) higher in EG7 PTK–treated wounds. The expression of mRNA encoding various growth factors, including *FGF2*, *FGF7*, epidermal growth factor (*EGF*), *IGF1*, *CTGF*, and *PDGF*, implicated in endothelial, fibroblast, and keratinocyte proliferation and migration (77), was significantly higher in EG7 PTK–treated wounds compared to those treated with NovoSorb at day 31 after treatment.

Deeper analysis of innate and adaptive immune cells within scaffold-infiltrating tissue showed significantly ($P < 0.001$) lower density of CD3-positive T cells in EG7 PTK–treated wounds compared to those treated with NovoSorb, suggesting resolution of the inflammatory wound healing phase along with decreased inflammation surrounding scaffold remnants (Fig. 7, A and B). Concurrently, we observed significantly lower density of CCR7-positive macrophages and FBGCs associated with PTK-UR scaffold remnants compared to NovoSorb, with CCR7 staining intensity varying as a function of distance from scaffold edge (Fig. 7, A and B). To further characterize the inflammatory response, we performed quantitative reverse transcription polymerase chain reaction (qRT-PCR) on bulk wound tissue samples. Relative to NovoSorb, EG7 PTK-UR samples were associated with significantly ($P < 0.05$) lower expression of proinflammatory genes such as interleukin-1β (*IL1B*) and *TNFA*. A similar decrease in expression of *CXCL8* and *CSF2*, as well as M1 macrophage marker *NOS2*, M2 macrophage marker arginase-1 (Arg-1) (fig. S15), and T_H1-specific transcription factor T-bet (*TBX21*), was observed within EG7 PTK–treated tissue compared to that treated with NovoSorb. Decreases in proinflammatory markers in EG7 PTK–treated wounds were accompanied by a concomitant up-regulation of anti-inflammatory markers such as T_H2 transcription factor *GATA3* and ILs including *IL10*, *IL13*, and *IL33* that have been implicated in type 2 immunity, tissue regeneration, and wound healing (78–82).

Enhanced wound closure, blood perfusion, and reepithelization of EG7 PTK-UR–treated porcine ischemic wounds

Ischemic wounds, such as those that can occur with venous leg ulcers, are associated with poor vasculature and delayed healing. To recapitulate slow-healing ischemic wounds in a porcine model, we used surgical cautery to create four raised bipedicle flaps in the dorsal region. Two 1 cm–by–1 cm excisional wounds were created in each of these flaps, which are separated from vascular sources from both the underlying muscle and the skin in either lateral direction (Fig. 8A) (35). We implanted these wounds with either EG7 PTK-UR or NovoSorb dermal matrices, and both wound closure (Fig. 8, B and C) and blood reperfusion (Fig. 8D) were measured over a period of 17 days. Wounds treated with EG7 PTK-UR scaffolds healed quickly, showing 76.1% closure over 17 days, compared to 8.3% for NovoSorb. In addition to the higher rate of wound closure, blood perfusion within EG7 PTK-UR–treated wounds was significantly higher ($P < 0.05$) at day 9 after surgery with gradual return to the perfusion flux values of unwounded skin within the ischemic flap (Fig. 8D). Similar to nonischemic wounds treated with NovoSorb, removal of the protective top layer disrupted wound bed granulation tissue, causing reinjury and stimulation of a secondary vascular response. At the study end point (day 17), EG7 PTK–treated wounds were significantly ($P < 0.05$) more reepithelialized as visualized and measured using CytoK14 IHC (Fig. 8, E and F). Examination of H&E- and trichrome-stained wound sections revealed significantly ($P < 0.05$) increased cellularity and inflammation surrounding NovoSorb scaffold remnants compared to EG7 PTK-UR scaffolds (Fig. 8G). Histopathological scoring revealed that EG7 PTK-UR showed higher epithelialization, lower inflammation, and higher overall wound healing score relative to NovoSorb BTM–treated wounds (Fig. 8, H and I). Increased inflammation within the granulation tissue of NovoSorb-treated wounds was visualized through MPO (Fig. 8J) and CCR7 (Fig. 8K)

IHC. NovoSorb scaffold remnants were surrounded by MPO^+ neutrophils, suggesting more persistent inflammation within these wounds, whereas EG7 PTK-UR showed few residual neutrophils at day 17. Similarly, $CCR7^+$ macrophages and FBGCs were observed at higher density in NovoSorb- treated wounds compared to those treated with EG7 PTK-UR. These data support that EG7 PTK-UR scaffolds are promising for treatment of skin wounds hindered by lack of vascular supply and provide consistent improvement over the benchmark NovoSorb BTM in multiple wound healing scenarios.

DISCUSSION

Chronic skin wounds are growing in prevalence and have a 40% chance of recurrence (3), emphasizing the need for low-cost and effective biodegradable dermal substitutes. Dermal substitutes provide immediate wound coverage without associated donor site morbidity, which is a major limitation for use of split-thickness autologous skin grafts. Application of cell-based dermal substitutes such as Apligraf to treat venous leg ulcers decreases median time to complete wound closure compared to standard of care (83), but use of a living cellular component decreases the shelf-life and increases production costs (84, 85). Animal-derived acellular scaffolds such as Integra BWM and OASIS ULTRA Tri-Layer Matrix can be stored at room temperature for long periods of time and have been successfully used to treat hard-to-heal wounds (14, 15). Integra BWM was initially indicated to treat burns in 2002 and has since been broadened for use in a variety of wound types. However, high cost [about $3855 per 10.16 × 12.7 cm graft (129 cm^2)] financially burdens the health care system and the patient. Complications, such as dehiscence, silicone detachment, hematoma, necrosis, and bacterial infection, resulting in poor integration of Integra BWM have also been reported in some instances to increase patient length of stay and total hospitalization cost (17). Synthetic scaffolds, especially PU-based foams, are a promising alternative that is more economical to manufacture at scale; the PU foam NovoSorb BTM is $850 for a 100-$cm^2$ product. However, PE-based materials are limited by an autocatalytic, hydrolytic degradation mechanism that proceeds independent of cellular activities (31). Autocatalytic degradation can cause rapid, mid- to late-stage material loss with consequent scaffold pore collapse, inhibition of cell infiltration, and poor wound stenting. More stable PE chemistries can be used to slow the degradation (86), but this approach increases the risk of developing a foreign body fibrous encapsulation response analogous to that caused by nondegradable implants (87).

To maximize the potential of synthetic scaffolds, overcome the shortcomings of PE-URs, and better elucidate structure-function relationships of PTK-URs, we synthesized a series of PTK diols with varied numbers of EG repeats between TK bonds in the polymer backbone. The goal was to tune this class of materials to harness ROS as a biological, cell-produced degradation mechanism (9) while, in turn, providing antioxidant properties, because oxidative stress is a characteristic of chronic wounds suffering from persistent type 1 immune response (88–90). A series of PTK diols was thus created to enable systematic evaluation of the effect of hydrophilicity on ROS-mediated scaffold degradation/ROS scavenging, immune response, vascularization, and quality of tissue repair. The EG7 formulation was more hydrophilic than any PTK-UR foams generated previously and emerged as the lead composition.

TK bond density and in vitro ROS reactivity showed an inverse correlation across the PTK-UR scaffold series. Decreased TK content with EG7, relative to the rest of the EG series, yielded a higher rate of degradation and mass loss, highlighting the importance of scaffold hydrophilicity on the rate of (oxidative) degradation. This is likely due to increased exposure and susceptibility of TK bonds to cleavage by strongly polar oxidative species in a hydrated environment. The differences in radical-scavenging potential between PTK-UR chemistries were diminished in organic solvents (DPPH assay performed in 80% ethanol) that more readily solvate the hydrophobic PTK-URs. It should be noted that, despite a similar overall EG content in EG2 and EG7 PTK scaffolds (20 versus 21 EG repeats per diol), significant ($P < 0.001$) differences in swelling ratio (208.72 versus 619.72% for EG2 and EG7, respectively) were observed. This is likely due to the inherent hydrophobicity of TK bonds and highlights the importance of having strongly hydrophilic spacer groups along the polymer backbone to ensure accessibility of the TK bond within aqueous environments. These results were also consistent with our previous observation that highly hydrated PEG- maleimide PTK hydrogels subcutaneously implanted in mice underwent oxidative degradation and facilitated effective tissue infiltration (36). The better ROS reactivity of the EG7 scaffolds in aqueous environments could also be connected to the theoretical log P values for the PTK diols; only the EG7 PTK diol chemistry showed a log P value below zero (indicating partition preference of water over octanol), whereas the remainder of the EG series had a log P value greater than 1. In vivo analysis of EG7 PTK-UR and 900t PE-UR shows significantly ($P < 0.01$) lower ROS concentration in TK-containing scaffold treatments in mice and reduction in 8-OhdG staining by IHC in histological wound samples from pigs. The reduced ROS concentration and cell damage in PTK scaffolds highlight the antioxidant properties of PTK-based foams. This likely contributes to the overall healing benefits observed with EG7 foams, because lowering oxidative stress can reduce nuclear factor κB–driven expression of inflammatory genes and cytokines that hinder nonhealing wounds (91, 92).

Differences in scaffold-tissue integration between EG0/EG1/EG2 PTK-UR scaffolds and EG7 PTK-URs were pronounced when implanted in porcine excisional skin wounds. Despite similarities in porosity, pore size, and dynamic mechanical compressive properties, all physical features that affect tissue response (45, 93, 94), EG7 PTK-UR scaffolds were more evenly distributed throughout the thickness of the wound (3.1 ± 0.4 mm), whereas there was lower tissue integration (<2 mm) of more hydrophobic PTK-UR scaffolds. This is likely due to a combination of scaffold swelling and degradation processes, which facilitate tissue infiltration into the foam pores. EG7 PTK-UR scaffolds had greater vascularization, which may be attributable not only to foam swelling/degradation but also to the relatively low expression of MPO, an antiangiogenic enzyme highly expressed in chronic wounds (95). EG7 PTK-URs were also associated with higher expression of growth factors such as PDGF (96, 97) and TGFB3 (98, 99), which positively affect endothelial cell proliferation, migration, and vessel maturation. In summary, we concluded that the favorable wound healing response of the EG7 versus the more hydrophobic PTK-UR scaffolds is related to mechanisms such as an improved biological response to the more swollen scaffold architecture, the composition of the protein adsorbate (63, 100), better ROS reactivity and scavenging, and faster breakdown and clearance of more hydrophilic PTK-UR material

degradation products. The EG7 PTK-UR scaffolds were also shown, similar to previous TK materials (34), to provide a relatively constant rate of in vivo breakdown without signs of an autocatalytic degradation mechanism, thereby mechanically supporting cell infiltration and slowly resorbing away within slow-to-heal wounds.

Another central finding of the study was that the EG7 PTK-UR biomaterial triggered a more desirable host immune response and time course of resolution relative to more hydrophobic PTK-URs. Tissue damage and biomaterial implantation are inextricably linked with initial extravasation of circulating neutrophils, monocytes, and macrophages to the site of injury (101). These inflammatory first responders generate ROS such as •OH, H_2O_2, ClO^-, and O_2^- as part of the innate immune response (102). The density of macrophages, T cells, and myofibroblasts, cell types responsible for nondegradable implant fibrous encapsulation (59, 61, 103), was all significantly ($P < 0.05$) decreased in the EG7 scaffold formulations. Active recruitment of neutrophils, monocytes, macrophages, and DCs to the site of biomaterial implantation can propagate inflammation and foreign body response, resulting in tissue and implant structural damage (104). We observed that EG7 PTK scaffolds were associated with significantly ($P < 0.05$) fewer CCR7-positive M1 macrophages and FBGCs relative to more hydrophobic PTK-URs. This agrees with previous observations that hydrophilic and anionic surfaces can cause biomaterial-adherent macrophage apoptosis and lower macrophage fusion, potentially limiting the deleterious effects of proinflammatory macrophages and reducing formation of FBGCs (105). DCs serve as an important bridge between innate and adaptive immunity by interacting with biomaterials through pathogen recognition receptors, leading to downstream antigen presentation and activation of T cells. Hydrophilic surfaces can also limit DC adhesion and maturation and consequently reduce proinflammatory T cell response (106, 107). Our subcutaneous implant mouse studies showed that EG7 PTK scaffolds had decreased number of infiltrating DCs compared to the more hydrophobic EG2 PTK-UR. These collective data suggest that the more hydrophobic scaffolds elicit a larger and more sustained inflammatory response compared to EG7 PTK-UR foams and that both initial recruitment and temporal evolution of the immune response have important implications in the wound healing potential of synthetic biomaterials.

Wound closure by reepithelialization is a key aspect of wound healing that is typically a primary outcome in clinical studies, because reestablishment of skin epidermal barrier is associated with reduced risk for infection and patient morbidity. A moist environment within chronic wounds has been linked with positive healing outcomes, as opposed to slower rates of wound closure and incomplete resurfacing seen in desiccated wounds (108). The ability of the EG7 PTK-UR to maintain a more hydrated wound environment may have also contributed to the significantly higher ($P < 0.01$) epithelial resurfacing of EG7 PTK–treated wounds compared to those treated with the more hydrophobic foams. In addition to the physical properties of EG7 PTK-UR foams, these scaffolds also recruited significantly higher (2.7-fold, $P < 0.001$) numbers of γδ T cells compared to EG2 PTK scaffolds when implanted in the mouse subcutaneous space. This T cell subpopulation stimulates secretion of growth factors (66) that promote keratinocyte migration and reepithelialization (53), several of which were up-regulated in EG7 PTK-UR–treated wounds [*IGF1* (twofold), *TGFB3* (twofold), and *PDGF* (threefold)].

To establish the therapeutic potential of the EG7 PTK-UR scaffolds more thoroughly in wound healing, we benchmarked against commercially available Integra BWM and NovoSorb BTM in pig skin wounds. Although similar rates of wound closure were observed between Integra and EG7 PTK-UR treatments, significantly ($P < 0.0001$) higher blood perfusion was seen in wounds treated with EG7 PTK-UR, indicating that neovascularization is a competitive advantage of EG7 PTK-UR scaffolds that may come more into play and yield superior performance relative to Integra for treatment of ischemic wounds. A slower degradation profile of NovoSorb was qualitatively inferred by the presence of a relatively large proportion of scaffold material in the wound after 31 days, which could potentially cause a prolonged host foreign body response. The persistence of NovoSorb in our studies was also consistent with previous observation of NovoSorb scaffold remnants in human skin biopsies taken 12 months after implantation (109). The relatively high in vivo stability of NovoSorb may at least partially explain the relatively higher expression of proinflammatory cytokine genes such as *IL1B* (3.1-fold), *TNFA* (2.1-fold), *NOS2* (4.5-fold), *CXCL8* (12-fold), and *CSF2* (5.9-fold) observed in NovoSorb-treated wounds compared to EG7 PTK-UR treatments. In comparison to architecturally and synthetically analogous NovoSorb foams, EG7 PTK-UR foams explanted from wounds at day 31 had significantly up-regulated expression of anti-inflammatory ILs *IL13* (2.8-fold) and *IL33* (3.2-fold), which are known to induce a tissue repair phenotype in macrophages (110, 111).

Unexpectedly, we observed significantly lower Arg-1 expression (10-fold), a marker often used to characterize the anti-inflammatory M2 macrophage phenotype, in EG7 PTK-UR–treated wounds relative to those treated with NovoSorb. Arg-1 IHC of wound tissue revealed lower but not the absence of Arg-1–expressing macrophages in EG7 PTK-UR–treated wounds. Intense Arg-1 staining was, however, observed colocalized with FBGCs surrounding NovoSorb scaffold remnants. Despite the importance of Arg-1 metabolism in macrophage polarization, elevated expression of Arg-1 has been reported in ischemic porcine wounds (112) and in human venous leg ulcers (112). In this context, high arginase activity has been linked to fibrosis (113), suggesting disparate biological ramifications of Arg-1–expressing macrophages. Related to the fibrosis phenotype, we observed a higher *TGFB3*/*TGFB1* expression ratio in EG7 PTK-UR–treated wounds compared to those treated with NovoSorb. It is known that *TGFB3* can promote scarless healing in mice, whereas up-regulated *TGFB1* is associated with excess ECM deposition and fibrosis (114).

To better recapitulate a clinical scenario with poorly healing skin wounds that would require treatment with a biomaterial, we used a previously optimized porcine model in which excisional wounds are created in raised flaps that are ischemic as a result of being surgically separated from the underlying fascia and lateral regions of skin (115). The raised skin flaps have reduced blood flow relative to surrounding normal skin as measured by Doppler imaging (35). This model captures aspects of ischemic-reperfusion injury, which can cause formation of chronic wounds in scenarios where there are underlying vascular insufficiencies (8). Ischemia-reperfusion triggers formation of free oxygen radicals that cause oxidative stress and cellular damage in the tissue. Thus, we chose this model as a promising platform for demonstrating the benefits of the antioxidant PTK-UR materials. In this model, both EG7 PTK-UR and NovoSorb scaffolds promoted cell infiltration, but EG7 PTK-UR scaffolds significantly improved the rate of wound closure and had higher percent

reepithelialization at the end point compared to NovoSorb. Treatment effect differences on reepithelialization between EG7 PTK-UR and NovoSorb BTM were better resolved compared to the nonischemic wound model. Similar to the wound healing profile seen in nonischemic wounds, EG7 PTK-UR treatment improved resolution of inflammation based on IHC for MPO-positive neutrophils and CCR7-positive macrophages. These data collectively suggest that the improved quality of tissue repair observed in full-thickness skin wounds on healthy pigs can be extended to ischemic skin wounds, a better recapitulation of chronic nonhealing phenotypes observed in patients.

There were some notable limitations of the promising studies presented here that will be considered in future product development work. First, testing the regenerative capacity of PTK-UR in acute wounds created on healthy pigs gives important but still limited insight into performance in chronic human skin wounds. Chronic wounds can be associated with more permanent ischemia, infection, and potentially higher oxidative stress that may overaccelerate the degradation of EG7 PTK-UR scaffolds. Additional tuning of mechanical properties to compensate for accelerated degradation may be required to effectively treat chronic wounds. The presence of a nondegradable, temporary membrane to create a bilaminar architecture such as that used in Integra and NovoSorb should also be a future consideration. Integration of an upper, removable layer on EG7 PTK-UR may help to better protect against moisture loss and bacterial infections as well as improve mechanical properties to reduce contraction of the underlying dermal layer. However, on the basis of our observation with NovoSorb, the ideal timing of the upper layer removal is also expected to be wound size and healing rate dependent and must be carefully monitored to ensure that the upper layer does not actually delay reepithelialization and slow closure. Another consideration is the small wound size used in the study. Reepithelization of larger wounds with EG7 PTK treatment alone may be challenging and would mostly likely be paired with the application of split-thickness skin graft or autologous keratinocyte transplant (116). The ischemic wound model used to study differences in PU scaffold–assisted wound healing of PTK-UR and NovoSorb matrices provides a robust model to study the healing kinetics of wounds with compromised vascularity. Although this model provides robust ischemia, it does not fully capture the background conditions that exist in many patients with chronic wounds (systemic vascular disease, diabetes, etc). It may be advantageous to carry out future studies using larger-sized excisional wounds or in animals with induced diabetes fed a high-fat diet before skin wounding.

In summary, we have developed a previously unidentified EG7 PTK-UR foam dressing that facilitates bulk tissue-scaffold integration, robust cellular and vascular infiltration, and wound resurfacing. These implants induce a moderate inflammatory response that effectively transitions to a prohealing phenotype, in addition to promoting ECM deposition, reepithelialization, and remodeling. When tested against clinically approved materials in porcine excisional wounds, EG7 PTK-UR had higher vascularization and similar wound closure to the gold-standard biologic material Integra BWM and significantly outperformed the synthetic PE-based foam NovoSorb.

MATERIALS AND METHODS

Study design

The current studies tested a library of ROS-degradable PTK-UR scaffolds in a porcine wound model. All surgical procedures were reviewed and approved by Vanderbilt University Institution and Animal Care and Use Committee. We created 28 2 cm–by–1 cm full-thickness wounds on the dorsal region of (healthy) adolescent Yorkshire female pigs (32 kg). Wounds were spaced ≥2 cm apart to avoid collateral effects while enabling screening of multiple biomaterial formulations (three to four wounds per treatment group), as previously reported (35, 117, 118). Treatment placement was randomized to avoid anatomical bias. To evaluate host response and early- to mid-stage immune response to the implanted scaffolds, pigs were euthanized, and wounds were harvested at 10 days after scaffold implantation. Full-thickness biopsies from within the wound margins were collected from anesthetized pigs before euthanasia for gene expression analysis. Wounds were harvested at 24 days after implant to further evaluate wound reepithelialization and other histological features within the PU (PE-UR controls and PTK-UR library) scaffolds (n = 6 to 10). In a third experiment, we treated porcine full-thickness wounds (n = 6 to 9) with our lead PTK-UR formulation, Integra BWM, and NovoSorb BTM and ended the study after 31 days. Wound closure and blood perfusion were noninvasively measured over the time course, whereas tissue samples for gene expression and histological evaluation were collected upon animal euthanasia. In a fourth experiment, four ischemic flaps were raised in a pig, and two 1 cm–by–1 cm wounds were created per flap. Wounds were randomized for treatment with either lead PTK-UR formulation or NovoSorb. Blood perfusion was measured over time before study end point (day 17), when wound tissues were harvested for histological analysis.

For all pig studies, the wound dressings were identical across all treatments and changed three times a week. Pigs received weekly antibiotic (Excede; Zoetis) injections to address potential bacterial infections, along with analgesics (Buprenex and fentanyl) to manage pain. Premature loss of scaffolds from the wounds due to mechanical disturbance by the animal before the predetermined end point was a criterion for exclusion of that sample from outcome analysis. Scoring of wound histology was done by a histopathologist blinded to the treatment. To further evaluate scaffold-infiltrating immune cell populations, we implanted two PU scaffolds (same PTK chemistry) in the ventral region of mice (n = 6 mice per scaffold type). Animals were then euthanized, and scaffolds were retrieved from the subcutaneous space at days 7, 14, and 21 after scaffold implantation. Cells were isolated from the explanted scaffolds (cells pooled from two scaffolds from the same animal) and profiled on the basis of cell surface and intracellular markers using flow cytometry. Mice were similarly implanted with 900t PE-UR and EG7 PTK-UR scaffolds to assess relative ROS levels associated with each scaffold chemistry in vivo, 4 days after implantation. All mice received analgesics (carprofen) every 24 hours for the first 72 hours after surgery to manage pain. None of the treatments resulted in animal weight loss or mortality during the experiment.

Statistical analysis

All analyses of qRT-PCR data were performed using dC_t values calculated from the geometric means of three housekeeping genes, *B2M*, *HPRT1*, and *RPL13A*. PTK treatment fold change (FC) and $\log_2$(FC) were calculated using $2^{-(dCt)}$ relative to 900t PE for each time point and presented as geometric mean and arithmetic mean, respectively. Heatmaps are presented as row-normalized dCt values or $\log_2$(FC) as indicated on each plot. For day 31 gene expression comparison, $\log_2$(FC) of EG7 PTK-UR is given relative to NovoSorb. One-way analyses of variance (ANOVAs) followed by Tukey's pairwise comparison were performed using GraphPad Prism to define statistical differences between treatments at a given time point. Kinetic studies were analyzed using two-way ANOVA between groups. Welch's *t* test was used to compare differences between two groups a given time point. Linear regression was used to analyze correlations between EG content and functional readouts including contact angle in vitro, tissue infiltration in vivo, and blood vessel density in vivo. Individual subject-level data are provided in data file S1.

Supplementary Material

Refer to Web version on PubMed Central for supplementary material.

Acknowledgments:

We acknowledge the Translational Pathology Shared Resource supported by National Cancer Institute (NCI)/NIH Cancer Center Support Grant 2P30 CA068485–14, Vanderbilt Mouse Metabolic Phenotyping Center Grant 5U24DK059637–13, and Digital Histology Shared Resources at Vanderbilt University.

Funding:

Funding was provided by the NIH through R01EB019409 and R01EB028690 and the NSF through DMR1349604 (CAREER) and GRFP DGE-1937963.

Data and materials availability:

All data associated with this study are present in the paper or the Supplementary Materials.

REFERENCES AND NOTES

1. Sen CK, Human wounds and its burden: An updated compendium of estimates. Adv. Wound Care (New Rochelle) 8, 39–48 (2019). [PubMed: 30809421]
2. Nussbaum SR, Carter MJ, Fife CE, DaVanzo J, Haught R, Nusgart M, Cartwright D, An economic evaluation of the impact, cost, and medicare policy implications of chronic nonhealing wounds. Value Health 21, 27–32 (2018). [PubMed: 29304937]
3. Frykberg RG, Banks J, Challenges in the treatment of chronic wounds. Adv. Wound Care (New Rochelle) 4, 560–582 (2015). [PubMed: 26339534]
4. Matoori S, Veves A, Mooney DJ, Advanced bandages for diabetic wound healing. Sci. Transl. Med. 13, eabe4839 (2021). [PubMed: 33731435]
5. Richmond NA, Maderal AD, Vivas AC, Evidence-based management of common chronic lower extremity ulcers. Dermatol. Ther. 26, 187–196 (2013). [PubMed: 23742279]
6. Jupiter DC, Thorud JC, Buckley CJ, Shibuya N, The impact of foot ulceration and amputation on mortality in diabetic patients. I: From ulceration to death, a systematic review. Int. Wound J. 13, 892–903 (2016). [PubMed: 25601358]

7. Rice TND, Hamblin MR, Herman IM, Acute and impaired wound healing: pathophysiology and current methods for drug delivery, part 1: Normal and chronic wounds: Biology, causes, and approaches to care. Adv. Skin Wound Care 25, 304–314 (2012). [PubMed: 22713781]
8. Peirce SM, Skalak TC, Rodeheaver GT, Ischemia-reperfusion injury in chronic pressure ulcer formation: A skin model in the rat. Wound Repair Regen. 8, 68–76 (2000). [PubMed: 10760216]
9. Mittal M, Siddiqui MR, Tran K, Reddy SP, Malik AB, Reactive oxygen species in inflammation and tissue injury. Antioxid. Redox Signal. 20, 1126–1167 (2014). [PubMed: 23991888]
10. Kirketerp-Moller K, Jensen PO, Fazli M, Madsen KG, Pedersen J, Moser C, Tolker-Nielsen T, Hoiby N, Givskov M, Bjarnsholt T, Distribution, organization, and ecology of bacteria in chronic wounds. J. Clin. Microbiol. 46, 2717–2722 (2008). [PubMed: 18508940]
11. Jones RE, Foster DS, Longaker MT, Management of chronic wounds-2018. JAMA 320, 1481–1482 (2018). [PubMed: 30326512]
12. Sheikholeslam M, Wright MEE, Jeschke MG, Amini-Nik S, Biomaterials for skin substitutes. Adv. Healthc. Mater. 7, 1700897 (2018).
13. Yannas IV, Burke JF, Orgill DP, Skrabut EM, Wound tissue can utilize a polymeric template to synthesize a functional extension of skin. Science 215, 174–176 (1982). [PubMed: 7031899]
14. Driver VR, Lavery LA, Reyzelman AM, Dutra TG, Dove CR, Kotsis SV, Kim HM, Chung KC, A clinical trial of integra template for diabetic foot ulcer treatment. Wound Repair Regen. 23, 891–900 (2015). [PubMed: 26297933]
15. Mostow EN, Haraway GD, Dalsing M, Hodde JP, King D; Group OVUS, Effectiveness of an extracellular matrix graft (OASIS Wound Matrix) in the treatment of chronic leg ulcers: A randomized clinical trial. J. Vasc. Surg. 41, 837–843 (2005). [PubMed: 15886669]
16. Kotler ED, Sharma V, Kang NV, Gareta EG, A universal classification system of skin substitutes inspired by factorial design. Tissue Eng. Part B Rev. 24, 279–288 (2018). [PubMed: 29336231]
17. Shakir S, Messa IV CA, Broach RB, Rhemtulla IA, Chatman B, D'Angelantonio A, Levin LS, Kovach III SJ, Serletti JM, Fischer JP, Indications and limitations of bilayer wound matrix-based lower extremity reconstruction: A multidisciplinary case-control study of 191 wounds. Plast. Reconstr. Surg. 145, 813–822 (2020). [PubMed: 32097330]
18. Li X, Cho B, Martin R, Seu M, Zhang C, Zhou Z, Choi JS, Jiang X, Chen L, Walia G, Yan J, Callanan M, Liu H, Colbert K, McAlmon JM, Grayson W, Reddy S, Sacks JM, Mao HQ, Nanofiber-hydrogel composite-mediated angiogenesis for soft tissue reconstruction. Sci. Transl. Med. 11, eaau6210 (2019). [PubMed: 31043572]
19. Clark AY, Martin KE, García JR, Johnson CT, Theriault HS, Han WM, Zhou DW, Botchwey EA, García AJ, Integrin-specific hydrogels modulate transplanted human bone marrow-derived mesenchymal stem cell survival, engraftment, and reparative activities. Nat. Commun. 11, 114 (2020). [PubMed: 31913286]
20. Zhu S, Li S, Escuin-Ordinas H, Dimatteo R, Xi W, Ribas A, Segura T, Accelerated wound healing by injectable star poly(ethylene glycol)-b-poly(propylene sulfide) scaffolds loaded with poorly water-soluble drugs. J. Control. Release 282, 156–165 (2018). [PubMed: 29751029]
21. Mir M, Ali MN, Barakullah A, Gulzar A, Arshad M, Fatima S, Asad M, Synthetic polymeric biomaterials for wound healing: A review. Prog. Biomater. 7, 1–21 (2018). [PubMed: 29446015]
22. Li A, Dearman BL, Crompton KE, Moore TG, Greenwood JE, Evaluation of a novel biodegradable polymer for the generation of a dermal matrix. J. Burn Care Res. 30, 717–728 (2009). [PubMed: 19506497]
23. MacEwan MR, MacEwan S, Wright AP, Kovacs TR, Batts J, Zhang L, Comparison of a fully synthetic electrospun matrix to a bi-layered xenograft in healing full thickness cutaneous wounds in a porcine model. Cureus 9, e1614 (2017). [PubMed: 29098126]
24. Fogh K, Nielsen J, Clinical utility of foam dressings in wound management: A review. Chron. Wound Care Manage. Res. 2015, 31–38 (2015).
25. Li L, Liu X, Niu Y, Ye J, Huang S, Liu C, Xu K, Synthesis and wound healing of alternating block polyurethanes based on poly(lactic acid) (PLA) and poly(ethylene glycol) (PEG). J. Biomed. Mater. Res. B Appl. Biomater. 105, 1200–1209 (2017). [PubMed: 27059634]

26. Laube T, Weisser J, Berger S, Borner S, Bischoff S, Schubert H, Gajda M, Brauer R, Schnabelrauch M, In situ foamable, degradable polyurethane as biomaterial for soft tissue repair. Korean J. Couns. Psychother. 78, 163–174 (2017).
27. Bonzani IC, Adhikari R, Houshyar S, Mayadunne R, Gunatillake P, Stevens MM, Synthesis of two-component injectable polyurethanes for bone tissue engineering. Biomaterials 28, 423–433 (2007). [PubMed: 16979756]
28. Adolph EJ, Pollins AC, Cardwell NL, Davidson JM, Guelcher SA, Nanney LB, Biodegradable lysine-derived polyurethane scaffolds promote healing in a porcine full-thickness excisional wound model. J. Biomater. Sci. Polym. Ed. 25, 1973–1985 (2014). [PubMed: 25290884]
29. Nelson CE, Kim AJ, Adolph EJ, Gupta MK, Yu F, Hocking KM, Davidson JM, Guelcher SA, Duvall CL, Tunable delivery of siRNA from a biodegradable scaffold to promote angiogenesis in vivo. Adv. Mater. 26, 607–614 (2014). [PubMed: 24338842]
30. Hafeman AE, Li B, Yoshii T, Zienkiewicz K, Davidson JM, Guelcher SA, Injectable biodegradable polyurethane scaffolds with release of platelet-derived growth factor for tissue repair and regeneration. Pharm. Res. 25, 2387–2399 (2008). [PubMed: 18516665]
31. Woodard LN, Grunlan MA, Hydrolytic degradation and erosion of polyester biomaterials. ACS Macro Lett. 7, 976–982 (2018). [PubMed: 30705783]
32. Ceonzo K, Gaynor A, Shaffer L, Kojima K, Vacanti CA, Stahl GL, Polyglycolic acid-induced inflammation: Role of hydrolysis and resulting complement activation. Tissue Eng. 12, 301–308 (2006). [PubMed: 16548688]
33. El-Mohtadi F, d'Arcy R, Tirelli N, Oxidation-responsive materials: Biological rationale, state of the art, multiple responsiveness, and open issues. Macromol. Rapid Commun. 40, e1800699 (2019). [PubMed: 30474897]
34. Martin JR, Gupta MK, Page JM, Yu F, Davidson JM, Guelcher SA, Duvall CL, A porous tissue engineering scaffold selectively degraded by cell-generated reactive oxygen species. Biomaterials 35, 3766–3776 (2014). [PubMed: 24491510]
35. Patil P, Martin JR, Sarett SM, Pollins AC, Cardwell NL, Davidson JM, Guelcher SA, Nanney LB, Duvall CL, Porcine ischemic wound-healing model for preclinical testing of degradable biomaterials. Tissue Eng. Part C Methods 23, 754–762 (2017). [PubMed: 28762881]
36. Martin JR, Patil P, Yu F, Gupta MK, Duvall CL, Enhanced stem cell retention and antioxidative protection with injectable, ROS-degradable PEG hydrogels. Biomaterials 263, 120377 (2020). [PubMed: 32947094]
37. Hafeman AE, Zienkiewicz KJ, Zachman AL, Sung HJ, Nanney LB, Davidson JM, Guelcher SA, Characterization of the degradation mechanisms of lysine-derived aliphatic poly(ester urethane) scaffolds. Biomaterials 32, 419–429 (2011). [PubMed: 20864156]
38. Zhang L, Cao Z, Bai T, Carr L, Ella-Menye JR, Irvin C, Ratner BD, Jiang S, Zwitterionic hydrogels implanted in mice resist the foreign-body reaction. Nat. Biotechnol. 31, 553–556 (2013). [PubMed: 23666011]
39. Wilson DS, Dalmasso G, Wang L, Sitaraman SV, Merlin D, Murthy N, Orally delivered thioketal nanoparticles loaded with TNF-α–siRNA target inflammation and inhibit gene expression in the intestines. Nat. Mater. 9, 923–928 (2010). [PubMed: 20935658]
40. Martin JR, Nelson CE, Gupta MK, Yu F, Sarett SM, Hocking KM, Pollins AC, Nanney LB, Davidson JM, Guelcher SA, Duvall CL, Local delivery of PHD2 siRNA from ROS-degradable scaffolds to promote diabetic wound healing. Adv. Healthc. Mater. 5, 2751–2757 (2016). [PubMed: 27717176]
41. Shim MS, Xia Y, A reactive oxygen species (ROS)-responsive polymer for safe, efficient, and targeted gene delivery in cancer cells. Angew. Chem. Int. Ed. Engl. 52, 6926–6929 (2013). [PubMed: 23716349]
42. Guimarães CF, Gasperini L, Marques AP, Reis RL, The stiffness of living tissues and its implications for tissue engineering. Nat. Rev. Mater. 5, 351–370 (2020).
43. Penuela L, Negro C, Massa M, Repaci E, Cozzani E, Parodi A, Scaglione S, Quarto R, Raiteri R, Atomic force microscopy for biomechanical and structural analysis of human dermis: A complementary tool for medical diagnosis and therapy monitoring. Exp. Dermatol. 27, 150–155 (2018). [PubMed: 29152798]

44. Liu B, Thayumanavan S, Mechanistic investigation on oxidative degradation of ros-responsive thioacetal/thioketal moieties and their implications. Cell Rep. Phys. Sci. 1, 100271 (2020).
45. Sussman EM, Halpin MC, Muster J, Moon RT, Ratner BD, Porous implants modulate healing and induce shifts in local macrophage polarization in the foreign body reaction. Ann. Biomed. Eng. 42, 1508–1516 (2014). [PubMed: 24248559]
46. Anderson JM, Rodriguez A, Chang DT, Foreign body reaction to biomaterials. Semin. Immunol. 20, 86–100 (2008). [PubMed: 18162407]
47. Ward WK, A review of the foreign-body response to subcutaneously-implanted devices: The role of macrophages and cytokines in biofouling and fibrosis. J. Diabetes Sci. Technol. 2, 768–777 (2008). [PubMed: 19885259]
48. Jhunjhunwala S, Neutrophils at the biological-material interface. ACS Biomater Sci. Eng. 4, 1128–1136 (2018). [PubMed: 33418651]
49. Selders GS, Fetz AE, Radic MZ, Bowlin GL, An overview of the role of neutrophils in innate immunity, inflammation and host-biomaterial integration. Regen Biomater. 4, 55–68 (2017). [PubMed: 28149530]
50. Valavanidis A, Vlachogianni T, Fiotakis C, 8-Hydroxy-2′-deoxyguanosine (8-OHdG): A critical biomarker of oxidative stress and carcinogenesis. J. Environ. Sci. Health C Environ. Carcinog. Ecotoxicol. Rev. 27, 120–139 (2009). [PubMed: 19412858]
51. Brown BN, Ratner BD, Goodman SB, Amar S, Badylak SF, Macrophage polarization: An opportunity for improved outcomes in biomaterials and regenerative medicine. Biomaterials 33, 3792–3802 (2012). [PubMed: 22386919]
52. Badylak SF, Valentin JE, Ravindra AK, McCabe GP, Stewart-Akers AM, Macrophage phenotype as a determinant of biologic scaffold remodeling. Tissue Eng. Part A 14, 1835–1842 (2008). [PubMed: 18950271]
53. Rousselle P, Braye F, Dayan G, Re-epithelialization of adult skin wounds: Cellular mechanisms and therapeutic strategies. Adv. Drug Deliv. Rev. 146, 344–365 (2019). [PubMed: 29981800]
54. Pastar I, Stojadinovic O, Yin NC, Ramirez H, Nusbaum AG, Sawaya A, Patel SB, Khalid L, Isseroff RR, Tomic-Canic M, Epithelialization in wound healing: A comprehensive review. Adv. Wound Care (New Rochelle) 3, 445–464 (2014). [PubMed: 25032064]
55. Usui ML, Mansbridge JN, Carter WG, Fujita M, Olerud JE, Keratinocyte migration, proliferation, and differentiation in chronic ulcers from patients with diabetes and normal wounds. J. Histochem. Cytochem. 56, 687–696 (2008). [PubMed: 18413645]
56. Sadtler K, Estrellas K, Allen BW, Wolf MT, Fan H, Tam AJ, Patel CH, Luber BS, Wang H, Wagner KR, Powell JD, Housseau F, Pardoll DM, Elisseeff JH, Developing a pro-regenerative biomaterial scaffold microenvironment requires T helper 2 cells. Science 352, 366–370 (2016). [PubMed: 27081073]
57. Strbo N, Yin N, Stojadinovic O, Innate and adaptive immune responses in wound epithelialization. Adv Wound Care (New Rochelle) 3, 492–501 (2014). [PubMed: 25032069]
58. MacLeod AS, Mansbridge JN, The innate immune system in acute and chronic wounds. Adv Wound Care (New Rochelle) 5, 65–78 (2016). [PubMed: 26862464]
59. Chung L, Maestas DR Jr., Lebid A, Mageau A, Rosson GD, Wu X, Wolf MT, Tam AJ, Vanderzee I, Wang X, Andorko JI, Zhang H, Narain R, Sadtler K, Fan H, Cihakova D, Le Saux CJ, Housseau F, Pardoll DM, Elisseeff JH, Interleukin 17 and senescent cells regulate the foreign body response to synthetic material implants in mice and humans. Sci. Transl. Med. 12, eaax3799 (2020). [PubMed: 32295900]
60. Harrison OJ, Linehan JL, Shih HY, Bouladoux N, Han SJ, Smelkinson M, Sen SK, Byrd AL, Enamorado M, Yao C, Tamoutounour S, Van Laethem F, Hurabielle C, Collins N, Paun A, Salcedo R, O'Shea JJ, Belkaid Y, Commensal-specific T cell plasticity promotes rapid tissue adaptation to injury. Science 363, eaat6280 (2019). [PubMed: 30523076]
61. Doloff JC, Veiseh O, Vegas AJ, Tam HH, Farah S, Ma M, Li J, Bader A, Chiu A, Sadraei A, Aresta-Dasilva S, Griffin M, Jhunjhunwala S, Webber M, Siebert S, Tang K, Chen M, Langan E, Dholokia N, Thakrar R, Qi M, Oberholzer J, Greiner DL, Langer R, Anderson DG, Colony stimulating factor-1 receptor is a central component of the foreign body response

to biomaterial implants in rodents and non-human primates. Nat. Mater. 16, 671–680 (2017). [PubMed: 28319612]

62. Li B, Yuan Z, Jain P, Hung H-C, He Y, Lin X, McMullen P, Jiang S, De novo design of functional zwitterionic biomimetic material for immunomodulation. Sci. Adv. 6, eaba0754 (2020). [PubMed: 32523997]
63. Visalakshan RM, MacGregor MN, Sasidharan S, Ghazaryan A, Mierczynska-Vasilev AM, Morsbach S, Mailander V, Landfester K, Hayball JD, Vasilev K, Biomaterial surface hydrophobicity-mediated serum protein adsorption and immune responses. ACS Appl. Mater. Interfaces 11, 27615–27623 (2019). [PubMed: 31310498]
64. Hsieh JY, Smith TD, Meli VS, Tran TN, Botvinick EL, Liu WF, Differential regulation of macrophage inflammatory activation by fibrin and fibrinogen. Acta Biomater. 47, 14–24 (2017). [PubMed: 27662809]
65. Gay D, Kwon O, Zhang Z, Spata M, Plikus MV, Holler PD, Ito M, Yang Z, Treffeisen E, Kim CD, Nace A, Zhang X, Baratono S, Wang F, Ornitz DM, Millar SE, Cotsarelis G, Fgf9 from dermal γδ T cells induces hair follicle neogenesis after wounding. Nat. Med. 19, 916–923 (2013). [PubMed: 23727932]
66. Jameson J, Ugarte K, Chen N, Yachi P, Fuchs E, Boismenu R, Havran WL, A role for skin γδ T cells in wound repair. Science 296, 747–749 (2002). [PubMed: 11976459]
67. Shook B, Xiao E, Kumamoto Y, Iwasaki A, Horsley V, CD301b^{+} macrophages are essential for effective skin wound healing. J. Invest. Dermatol. 136, 1885–1891 (2016). [PubMed: 27287183]
68. Sommerfeld SD, Cherry C, Schwab RM, Chung L, Maestas DR, Laffont P, Stein JE, Tam A, Ganguly S, Housseau F, Taube JM, Pardoll DM, Cahan P, Elisseeff JH, Interleukin-36γ–producing macrophages drive IL-17-mediated fibrosis. Sci Immunol 4, eaax4783 (2019). [PubMed: 31604843]
69. Shook BA, Wasko RR, Gonzalez GCR, Gatzimas ES, Giraldez FL, Dash BC, Munoz-Rojas AR, Aultman KD, Zwick RK, Lei V, Arbiser JL, Jensen KM, Clark DA, Hsia HC, Horsley V, Myofibroblast proliferation and heterogeneity are supported by macrophages during skin repair. Science 362, (2018).
70. Koivisto L, Heino J, Hakkinen L, Larjava H, Integrins in wound healing. Adv. Wound Care (New Rochelle) 3, 762–783 (2014). [PubMed: 25493210]
71. Switala-Jelen K, Dabrowska K, Opolski A, Lipinska L, Nowaczyk M, Gorski A, The biological functions of beta3 integrins. Folia Biol (Praha) 50, 143–152 (2004). [PubMed: 15581065]
72. Akhurst RJ, Hata A, Targeting the TGFβ signalling pathway in disease. Nat. Rev. Drug Discov. 11, 790–811 (2012). [PubMed: 23000686]
73. Nagase H, Visse R, Murphy G, Structure and function of matrix metalloproteinases and TIMPs. Cardiovasc. Res. 69, 562–573 (2006). [PubMed: 16405877]
74. Caley MP, Martins VL, O'Toole EA, Metalloproteinases and wound healing. Adv. Wound Care (New Rochelle) 4, 225–234 (2015). [PubMed: 25945285]
75. Vaalamo M, Mattila L, Johansson N, Kariniemi AL, Karjalainen-Lindsberg ML, Kahari VM, Saarialho-Kere U, Distinct populations of stromal cells express collagenase-3 (MMP-13) and collagenase-1 (MMP-1) in chronic ulcers but not in normally healing wounds. J. Invest. Dermatol. 109, 96–101 (1997). [PubMed: 9204962]
76. Vaalamo M, Leivo T, Saarialho-Kere U, Differential expression of tissue inhibitors of metalloproteinases (TIMP-1, −2, −3, and −4) in normal and aberrant wound healing. Hum. Pathol. 30, 795–802 (1999). [PubMed: 10414498]
77. Barrientos S, Stojadinovic O, Golinko MS, Brem H, Tomic-Canic M, PERSPECTIVE ARTICLE: Growth factors and cytokines in wound healing. Wound Repair Regen. 16, 585–601 (2008). [PubMed: 19128254]
78. Molofsky AB, Savage AK, Locksley RM, Interleukin-33 in tissue homeostasis, injury, and inflammation. Immunity 42, 1005–1019 (2015). [PubMed: 26084021]
79. Li T, Zhang Z, Bartolacci JG, Dwyer GK, Liu Q, Mathews LR, Velayutham M, Roessing AS, Lee YC, Dai H, Shiva S, Oberbarnscheidt MH, Dziki JL, Mullet SJ, Wendell SG, Wilkinson JD, Webber SA, Trageser MW, Watkins SC, Demetris AJ, Hussey GS, Badylak SF, Turnquist HR,

Graft IL-33 regulates infiltrating macrophages to protect against chronic rejection. J. Clin. Invest. 130, 5397–5412 (2020). [PubMed: 32644975]

80. Bosurgi L, Cao YG, Cabeza-Cabrerizo M, Tucci A, Hughes LD, Kong Y, Weinstein JS, Licona-Limon P, Schmid ET, Pelorosso F, Gagliani N, Craft JE, Flavell RA, Ghosh S, Rothlin CV, Macrophage function in tissue repair and remodeling requires IL-4 or IL-13 with apoptotic cells. Science 356, 1072–1076 (2017). [PubMed: 28495875]
81. Gieseck III RL, Wilson MS, Wynn TA, Type 2 immunity in tissue repair and fibrosis. Nat. Rev. Immunol. 18, 62–76 (2018). [PubMed: 28853443]
82. Griffin DR, Archang MM, Kuan CH, Weaver WM, Weinstein JS, Feng AC, Ruccia A, Sideris E, Ragkousis V, Koh J, Plikus MV, Di Carlo D, Segura T, Scumpia PO, Activating an adaptive immune response from a hydrogel scaffold imparts regenerative wound healing. Nat. Mater. 20, 560–569 (2020). [PubMed: 33168979]
83. Sabolinski ML, Gibbons G, Comparative effectiveness of a bilayered living cellular construct and an acellular fetal bovine collagen dressing in the treatment of venous leg ulcers. J. Comp. Eff. Res. 7, 797–805 (2018). [PubMed: 29809059]
84. Zaulyanov L, Kirsner RS, A review of a bi-layered living cell treatment (Apligraf) in the treatment of venous leg ulcers and diabetic foot ulcers. Clin. Interv. Aging 2, 93–98 (2007). [PubMed: 18044080]
85. Samsell B, McLean J, Cazzell S, Dorsch K, Moyer PM, Moore M, Health economics for treatment of diabetic foot ulcers: A cost-effectiveness analysis of eight skin substitutes. J. Wound Care 28, S14–S26 (2019).
86. Zhang H, Zhou L, Zhang W, Control of scaffold degradation in tissue engineering: A review. Tissue Eng. Part B Rev. 20, 492–502 (2014). [PubMed: 24547761]
87. Alijotas-Reig J, Fernández-Figueras MT, Puig L, Late-onset inflammatory adverse reactions related to soft tissue filler injections. Clin. Rev. Allergy Immunol. 45, 97–108 (2013). [PubMed: 23361999]
88. Moseley R, Hilton JR, Waddington RJ, Harding KG, Stephens P, Thomas DW, Comparison of oxidative stress biomarker profiles between acute and chronic wound environments. Wound Repair Regen. 12, 419–429 (2004). [PubMed: 15260807]
89. James TJ, Hughes MA, Cherry GW, Taylor RP, Evidence of oxidative stress in chronic venous ulcers. Wound Repair Regen. 11, 172–176 (2003). [PubMed: 12753597]
90. Schafer M, Werner S, Oxidative stress in normal and impaired wound repair. Pharmacol. Res. 58, 165–171 (2008). [PubMed: 18617006]
91. Forrester SJ, Kikuchi DS, Hernandes MS, Xu Q, Griendling KK, Reactive oxygen species in metabolic and inflammatory signaling. Circ. Res. 122, 877–902 (2018). [PubMed: 29700084]
92. Dunnill C, Patton T, Brennan J, Barrett J, Dryden M, Cooke J, Leaper D, Georgopoulos NT, Reactive oxygen species (ROS) and wound healing: The functional role of ROS and emerging ROS-modulating technologies for augmentation of the healing process. Int. Wound J. 14, 89–96 (2017). [PubMed: 26688157]
93. Blakney AK, Swartzlander MD, Bryant SJ, The effects of substrate stiffness on the in vitro activation of macrophages and in vivo host response to poly(ethylene glycol)-based hydrogels. J. Biomed. Mater. Res. A 100, 1375–1386 (2012). [PubMed: 22407522]
94. Walthers CM, Nazemi AK, Patel SL, Wu BM, Dunn JC, The effect of scaffold macroporosity on angiogenesis and cell survival in tissue-engineered smooth muscle. Biomaterials 35, 5129–5137 (2014). [PubMed: 24695092]
95. Krisp C, Jacobsen F, McKay MJ, Molloy MP, Steinstraesser L, Wolters DA, Proteome analysis reveals antiangiogenic environments in chronic wounds of diabetes mellitus type 2 patients. Proteomics 13, 2670–2681 (2013). [PubMed: 23798543]
96. Stratman AN, Schwindt AE, Malotte KM, Davis GE, Endothelial-derived PDGF-BB and HB-EGF coordinately regulate pericyte recruitment during vasculogenic tube assembly and stabilization. Blood 116, 4720–4730 (2010). [PubMed: 20739660]
97. Cao R, Brakenhielm E, Pawliuk R, Wariaro D, Post MJ, Wahlberg E, Leboulch P, Cao Y, Angiogenic synergism, vascular stability and improvement of hind-limb ischemia by a combination of PDGF-BB and FGF-2. Nat. Med. 9, 604–613 (2003). [PubMed: 12669032]

98. Carmeliet P, Angiogenesis in health and disease. Nat. Med. 9, 653–660 (2003). [PubMed: 12778163]

99. Muraoka N, Shum L, Fukumoto S, Nomura T, Ohishi M, Nonaka K, Transforming growth factor-β3 promotes mesenchymal cell proliferation and angiogenesis mediated by the enhancement ofcyclin D1,Flk-1, andCD31 gene expression during CL/Fr mouse lip fusion. Birth Defects Res. A Clin. Mol. Teratol. 73, 956–965 (2005). [PubMed: 16323168]

100. Lv L, Xie Y, Li K, Hu T, Lu X, Cao Y, Zheng X, Unveiling the mechanism of surface hydrophilicity-modulated macrophage polarization. Adv. Healthc. Mater. 7, e1800675 (2018). [PubMed: 30106513]

101. Eming SA, Hammerschmidt M, Krieg T, Roers A, Interrelation of immunity and tissue repair or regeneration. Semin. Cell Dev. Biol. 20, 517–527 (2009). [PubMed: 19393325]

102. Dupré-Crochet S, Erard M, Nüβe O, ROS production in phagocytes: Why, when, and where? J. Leukoc. Biol. 94, 657–670 (2013). [PubMed: 23610146]

103. Veiseh O, Doloff JC, Ma M, Vegas AJ, Tam HH, Bader AR, Li J, Langan E, Wyckoff J, Loo WS, Jhunjhunwala S, Chiu A, Siebert S, Tang K, Hollister-Lock J, Aresta-Dasilva S, Bochenek M, Mendoza-Elias J, Wang Y, Qi M, Lavin DM, Chen M, Dholakia N, Thakrar R, Lacik I, Weir GC, Oberholzer J, Greiner DL, Langer R, Anderson DG, Size- and shape-dependent foreign body immune response to materials implanted in rodents and non-human primates. Nat. Mater. 14, 643–651 (2015). [PubMed: 25985456]

104. Veiseh O, Vegas AJ, Domesticating the foreign body response: Recent advances and applications. Adv. Drug Deliv. Rev. 144, 148–161 (2019). [PubMed: 31491445]

105. Brodbeck WG, Patel J, Voskerician G, Christenson E, Shive MS, Nakayama Y, Matsuda T, Ziats NP, Anderson JM, Biomaterial adherent macrophage apoptosis is increased by hydrophilic and anionic substrates in vivo. Proc. Natl. Acad. Sci. U.S.A. 99, 10287–10292 (2002). [PubMed: 12122211]

106. Keselowsky BG, Lewis JS, Dendritic cells in the host response to implanted materials. Semin. Immunol. 29, 33–40 (2017). [PubMed: 28487131]

107. Park J, Babensee JE, Differential functional effects of biomaterials on dendritic cell maturation. Acta Biomater. 8, 3606–3617 (2012). [PubMed: 22705044]

108. Winter GD, Formation of the scab and the rate of epithelization of superficial wounds in the skin of the young domestic pig. Nature 193, 293–294 (1962). [PubMed: 14007593]

109. Dearman BL, Li A, Greenwood JE, Optimization of a polyurethane dermal matrix and experience with a polymer-based cultured composite skin. J. Burn Care Res. 35, 437–448 (2014). [PubMed: 24823336]

110. Gordon S, Alternative activation of macrophages. Nat. Rev. Immunol. 3, 23–35 (2003). [PubMed: 12511873]

111. Van Dyken SJ, Nussbaum JC, Lee J, Molofsky AB, Liang HE, Pollack JL, Gate RE, Haliburton GE, Ye CJ, Marson A, Erle DJ, Locksley RM, A tissue checkpoint regulates type 2 immunity. Nat. Immunol. 17, 1381–1387 (2016). [PubMed: 27749840]

112. Roy S, Biswas S, Khanna S, Gordillo G, Bergdall V, Green J, Marsh CB, Gould LJ, Sen CK, Characterization of a preclinical model of chronic ischemic wound. Physiol. Genomics 37, 211–224 (2009). [PubMed: 19293328]

113. Abd-El-Aleem SA, Ferguson MW, Appleton I, Kairsingh S, Jude EB, Jones K, McCollum CN, Ireland GW, Expression of nitric oxide synthase isoforms and arginase in normal human skin and chronic venous leg ulcers. J. Pathol. 191, 434–442 (2000). [PubMed: 10918219]

114. Shah M, Foreman DM, Ferguson MW, Neutralisation of TGF-beta 1 and TGF-beta 2 or exogenous addition of TGF-beta 3 to cutaneous rat wounds reduces scarring. J. Cell Sci. 108, 985–1002 (1995). [PubMed: 7542672]

115. Kalani M, Brismar K, Fagrell B, Ostergren J, Jorneskog G, Transcutaneous oxygen tension and toe blood pressure as predictors for outcome of diabetic foot ulcers. Diabetes Care 22, 147–151 (1999). [PubMed: 10333917]

116. Larson KW, Austin CL, Thompson SJ, Treatment of a full-thickness burn injury with novosorb biodegradable temporizing matrix and RECELL autologous skin cell suspension: A case series. J. Burn Care Res. 41, 215–219 (2020). [PubMed: 31765469]

117. Shen YI, Song HG, Papa A, Burke J, Volk SW, Gerecht S, Acellular hydrogels for regenerative burn wound healing: Translation from a porcine model. J. Invest. Dermatol. 135, 2519–2529 (2015). [PubMed: 26358387]

118. Puthia M, Butrym M, Petrlova J, Stromdahl AC, Andersson MA, Kjellstrom S, Schmidtchen A, A dual-action peptide-containing hydrogel targets wound infection and inflammation. Sci. Transl. Med. 12, eaax6601 (2020). [PubMed: 31894104]

119. Martin JR, Howard MT, Wang S, Berger AG, Hammond PT, Oxidation-responsive, tunable growth factor delivery from polyelectrolyte-coated implants. Adv. Healthc. Mater. 10, e2001941 (2021). [PubMed: 33738985]

120. Yang H, Morris JJ, Lopina ST, Polyethylene glycol-polyamidoamine dendritic micelle as solubility enhancer and the effect of the length of polyethylene glycol arms on the solubility of pyrene in water. J. Colloid Interface Sci. 273, 148–154 (2004). [PubMed: 15051444]

121. Li B, Davidson JM, Guelcher SA, The effect of the local delivery of platelet-derived growth factor from reactive two-component polyurethane scaffolds on the healing in rat skin excisional wounds. Biomaterials 30, 3486–3494 (2009). [PubMed: 19328544]

122. Moghimi A, Omrani I, Nabid MR, Mahmoodi M, Quantification of hydroxyl group in polymers containing trace water by 19F NMR spectroscopy. Eur. Polym. J. 49, 228–234 (2013).

123. Yao Y, Ding J, Wang Z, Zhang H, Xie J, Wang Y, Hong L, Mao Z, Gao J, Gao C, ROS-responsive polyurethane fibrous patches loaded with methylprednisolone (MP) for restoring structures and functions of infarcted myocardium in vivo. Biomaterials 232, 119726 (2020). [PubMed: 31901502]

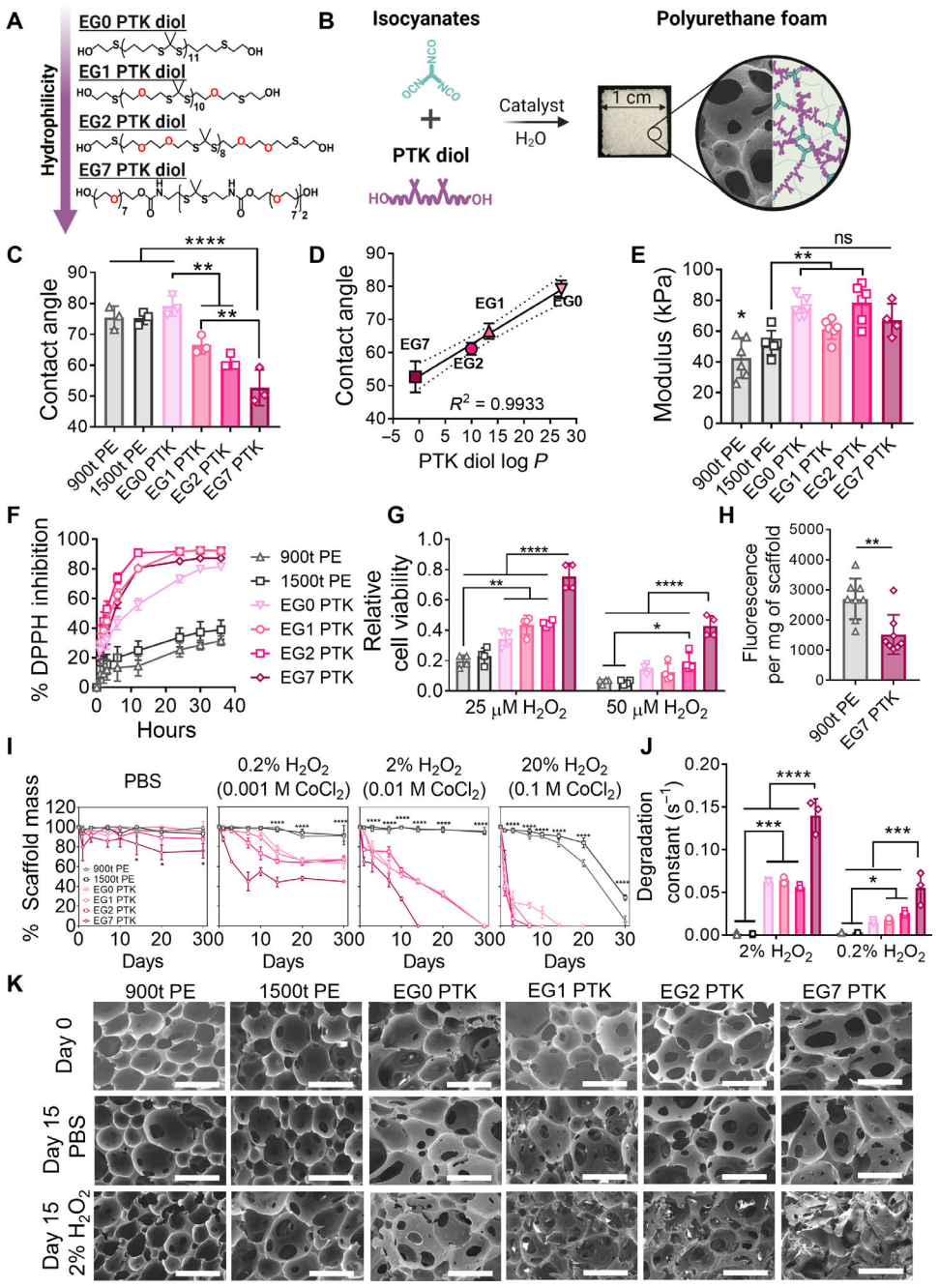

Fig. 1. Increasing EG content within PTK diols increases PU scaffold hydrophilicity and radical reactivity.

(**A**) Chemical structures showing controlled variation of the number (0 to 7) of ethylene glycol (EG) units in the polythioketal (PTK) diol backbone. (**B**) Reactive liquid molding of isocyanates and PTK diols yields covalently cross-linked three-dimensional PU networks with interconnected pores (scanning electron microscopy image) that permit cell infiltration. (**C**) Urethane (UR) film contact angle measurements and (**D**) correlation between measured contact angles and computed PTK diol log *P* values (ChemAxon). (**E**) UR scaffold modulus measured under compression under hydrated, aqueous conditions. (**F**) Radical scavenging

capacity of PTK-UR compared to PE-UR scaffolds measured through DPPH inhibition. (**G**) Cytoprotective properties of PTK diols (matched TK content) determined after cell (NIH 3T3 fibroblasts) exposure to 25 or 50 μM H_2O_2 for 24 hours. (**H**) Ex vivo H_2O_2 concentration measured within polyester-urethane (PE-UR) and EG7 PTK-UR scaffolds explanted from the subcutaneous space in mice using Amplex Red. (**I**) Scaffold mass loss over 30 days in PBS, 0.2% H_2O_2 in 0.001 M $CoCl_2$, 2% H_2O_2 in 0.01 M $CoCl_2$, or 20% H_2O_2 in 0.1 M $CoCl_2$ at 37°C. (**J**) Degradation constants derived from the experimental data. (**K**) Scanning electron microscopy images of PTK-UR scaffolds incubated in PBS or 2% H_2O_2/0.01 M $CoCl_2$ at days 0 and 15. Scale bars, 200 μm. Data are presented as means ± SD, $n = 3$ to 4 scaffolds. ns, not significant. *$P < 0.05$, **$P < 0.01$, ***$P < 0.001$, and ****$P < 0.0001$, by analysis of variance (ANOVA).

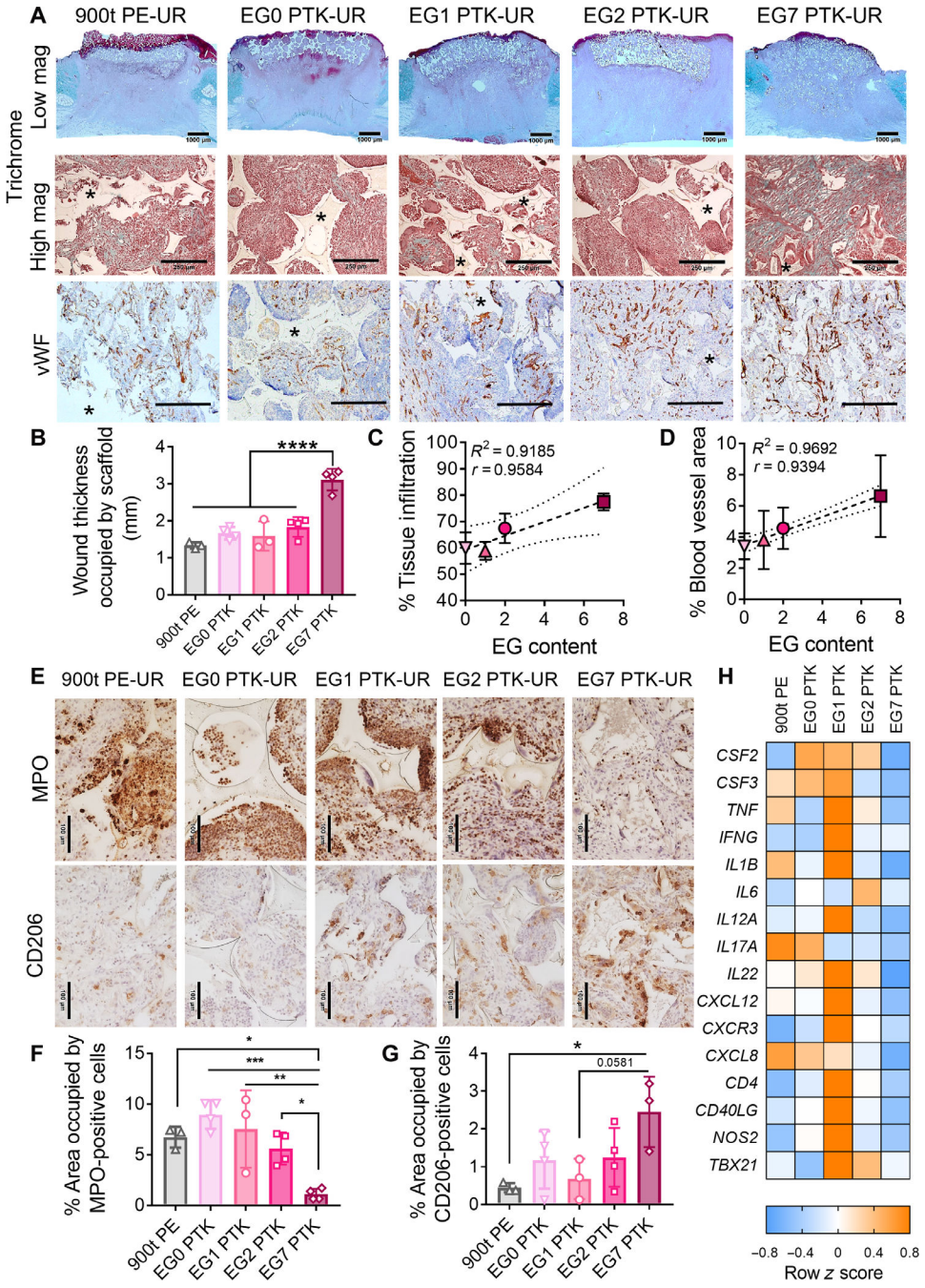

Fig. 2. Pig skin wound 10 days after implantation: Hydrophilic EG7 PTK-UR chemistry shows better wound bed integration and neovascularization and a less proinflammatory wound microenvironment.

(**A**) Representative trichrome images showing bulk integration of scaffold within the wound bed (low magnification, scale bars, 1000 μm) and cellular infiltration and extracellular matrix (ECM) deposition within scaffold pores (high magnification, scale bars, 250 μm). vWF immunohistochemistry (IHC) shows vascularization (brown) within the scaffold-infiltrating granulation tissue. Scale bars, 250 μm. Asterisks indicate scaffold remnants. (**B**) Quantification of bulk scaffold integration measured as wound thickness occupied by

scaffolds. Correlation between PTK diol EG content and percent tissue infiltration within the scaffold pores (**C**) and PTK diol EG content and blood vessel area (**D**). (**E**) Representative MPO (neutrophils) and CD206 (M2 macrophages) IHC images of scaffold-infiltrating tissue. Scale bars, 100 μm. Quantified staining at day 10 for (**F**) MPO^+ neutrophils and (**G**) $CD206^+$ macrophages. (**H**) Bulk tissue gene expression analysis of inflammatory mediators in porcine skin wound bed 10 days after scaffold implantation. Color-coded heatmap showing row-normalized *z* scores ($n = 4$ wounds per group) of inflammatory marker gene expression. Data are presented as means ± SD, $n = 3$ to 4 wounds, ANOVA, $^*P < 0.05$, $^{**}P < 0.01$, $^{***}P < 0.001$, and $^{****}P < 0.0001$.

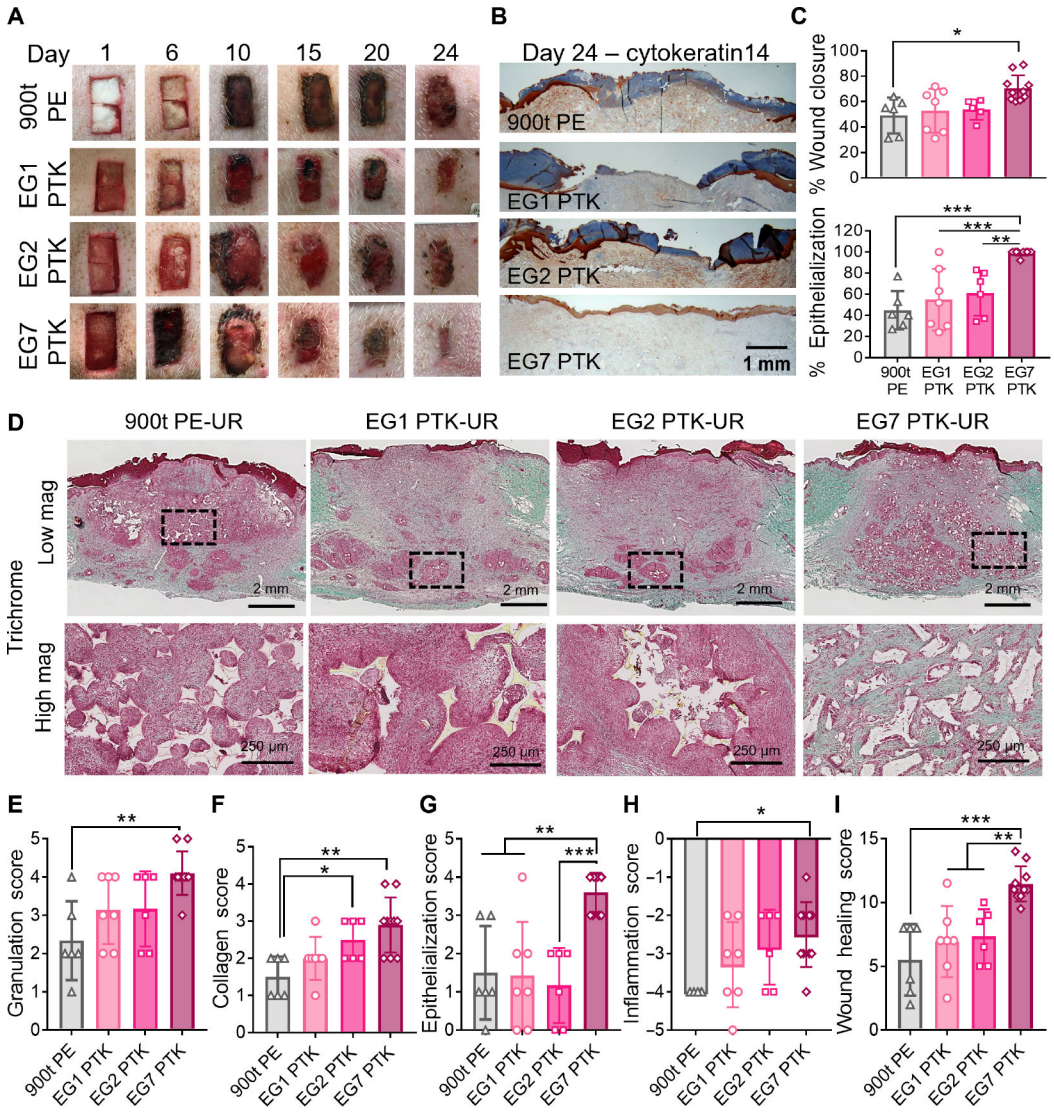

Fig. 3. EG7 PTK-UR shows complete reepithelization and overall enhanced wound healing than more hydrophobic scaffolds in day 24 pig skin wounds.

(**A**) Representative images showing scaffold implantation and wound resolution over a period of 24 days. (**B**) Representative cytokeratin14 IHC showing wound reepithelialization. (**C**) Wound closure measurements. Top: Quantified wound area (day 24) relative to initial wound size (day 0). Bottom: Percentage of wound length covered by cytokeratin14^{+} (CytK14^{+}) keratinocytes. (**D**) Representative trichrome images of granulation tissue analyzed 24 days after scaffold implantation (low magnification, scale bars, 2 mm; high magnification, scale bars, 250 μm). Wound score was assessed through treatment-blinded histopathologist analysis of trichrome and H&E images for (**E**) granulation tissue, (**F**) collagen deposition, (**G**) epithelialization, and (**H**) inflammation, yielding (**I**) a cumulative wound healing score for each scaffold type tested. Data are presented as means ± SD, $n = 6$ to 10 wounds, $^{*}P < 0.05$, $^{**}P < 0.01$, and $^{***}P < 0.001$, by ANOVA.

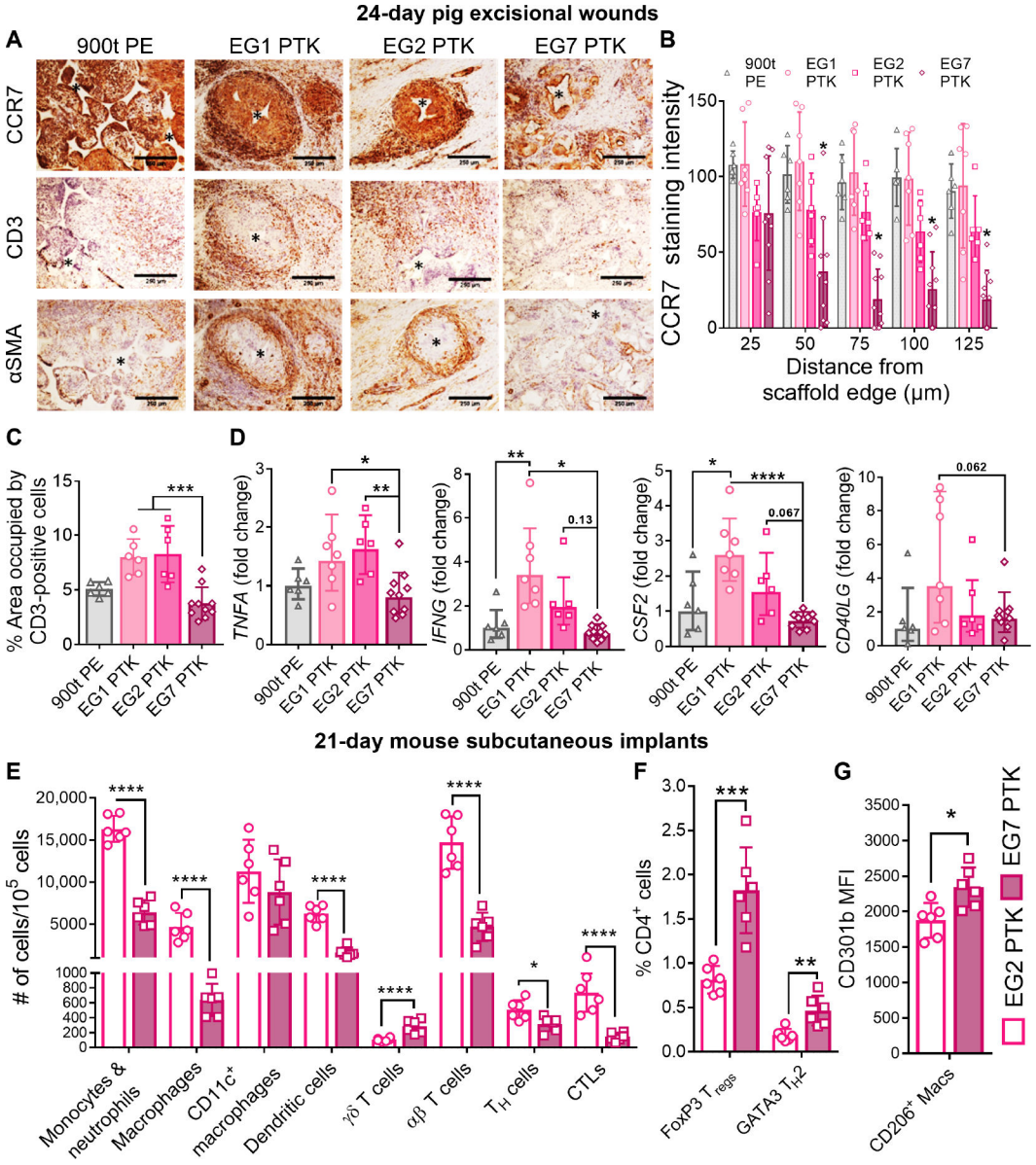

Fig. 4. EG7 PTK-UR scaffolds elicit a less proinflammatory immune phenotype relative to more hydrophobic variants in day 24 pig skin wounds and day 21 mouse subcutaneous implants.

(**A**) CCR7, CD3, and αSMA IHC of pig excisional skin wounds 24 days after treatment. Scale bars, 250 μm. (**B**) Quantification of CCR7 staining intensity as a function of distance from scaffold remnant edges. (**C**) Quantification of $CD3^+$pixel area within the wound. (**D**) qRT-PCR quantification of the expression of proinflammatory genes *TNFA*, *IFNG*, *CSF2*, and *CD40LG* within pig wound scaffolds at day 24. (**E**) Scaffold-infiltrating myeloid and lymphoid populations quantified 21 days after subcutaneous implantation of EG2 PTK (empty bars) and EG7 PTK (pink filled bars) scaffolds in mice. (**F**) Percentage of $FOXP3^+$ and $GATA3^+$ infiltrating CD4 helper T cells in EG2 versus EG7 scaffolds. (**G**) Expression of CD301b in EG7 scaffold–infiltrating $CD206^+$ macrophages compared to EG2 PTK scaffolds. Data are presented as means ± SD, $n = 6$ to 10 wounds, $^*P < 0.05$, $^{**}P < 0.01$, $^{***}P < 0.001$, and $^{****}P < 0.0001$, by ANOVA. MFI, mean fluorescence intensity.

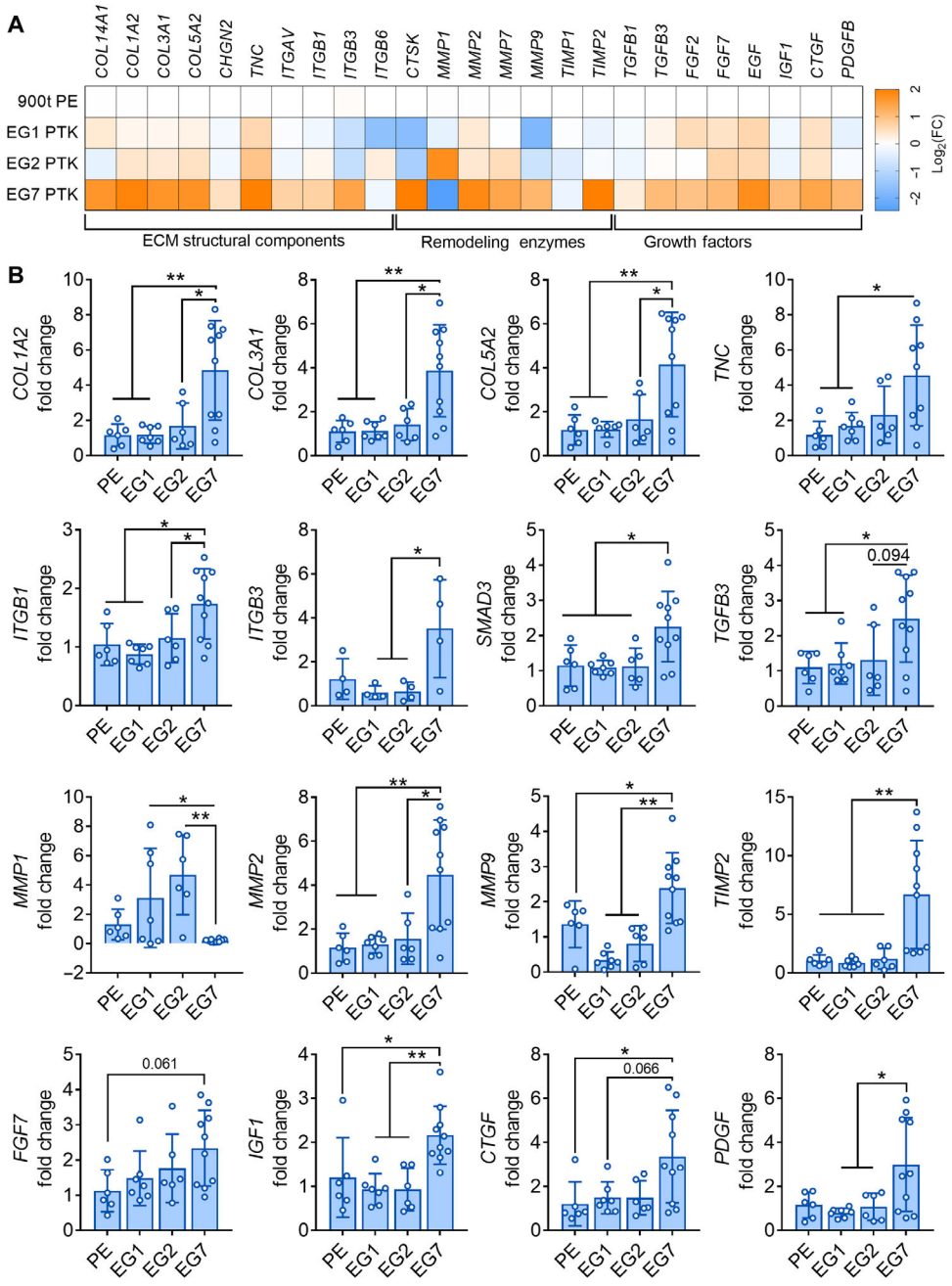

Fig. 5. EG7 PTK-UR scaffolds promote higher expression of progrowth, ECM, and remodeling genes relative to more hydrophobic scaffolds in day 24 porcine wounds.

(**A**) Bulk tissue differential gene expression of genes encoding ECM components, remodeling enzymes, and growth factors 24 days after wound. Gene expression was analyzed and displayed as color-coded heatmap showing $\log_2$(FC) relative to PE 900t control. (**B**) Expression fold change (FC) of selected genes relative to 900t PE–treated wounds. Data are presented as means ± SD, $n = 4$ to 10 wounds, $^*P < 0.05$, and $^{**}P < 0.01$, by ANOVA.

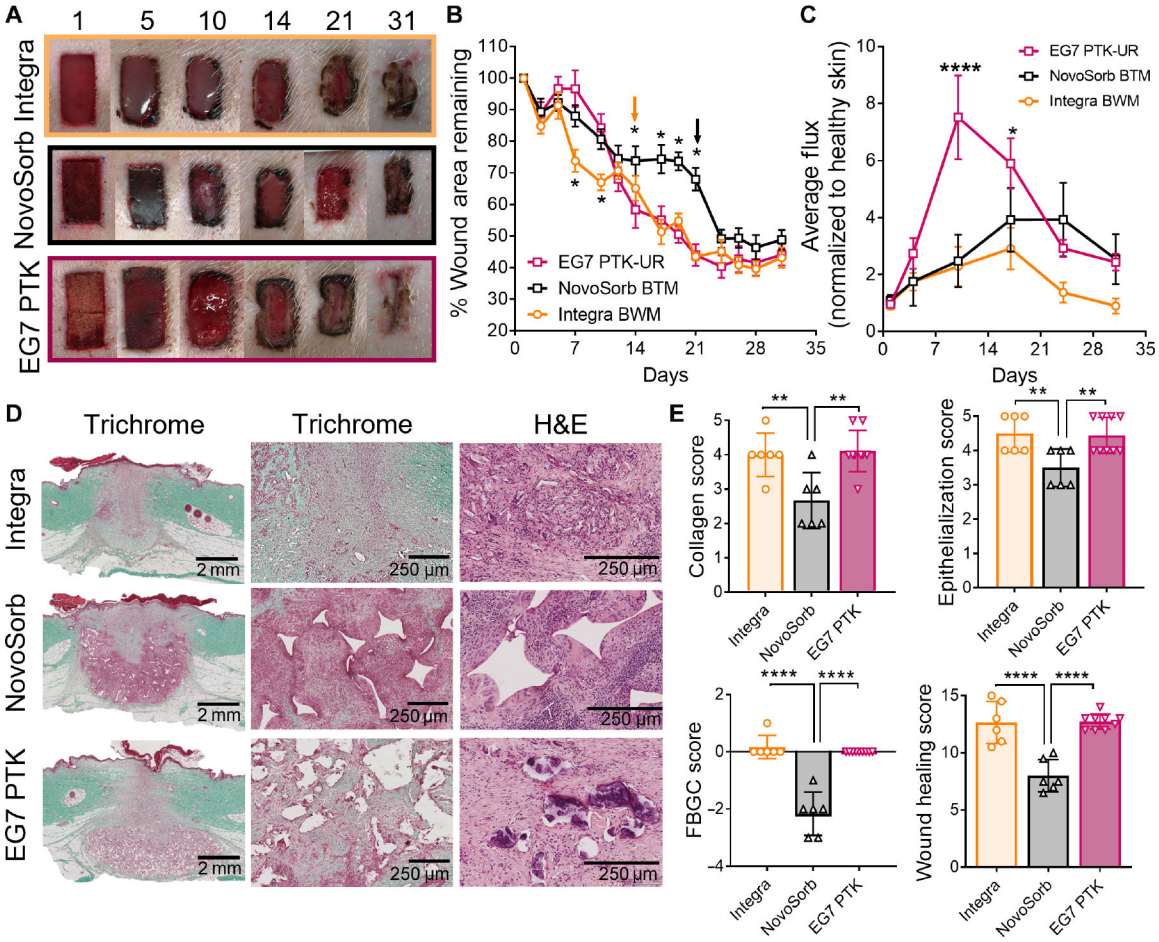

Fig. 6. EG7 PTK-UR scaffold wound healing benchmarking versus Integra BWM and NovoSorb BTM in day 31 pig excisional wounds.

(**A**) Images showing scaffold implantation and temporal closure of 2 cm–by–1 cm porcine skin wounds treated with collagen-based Integra Bilayer Wound Matrix (BWM), PE-based NovoSorb Biodegradable Temporizing Matrix (BTM), or EG7 PTK-UR foams. (**B**) Kinetics of wound closure. Arrows indicate time point of manufacturer-recommended removal of protective layer from Integra and NovoSorb. (**C**) Relative blood perfusion within scaffold-bearing wounds measured by laser Doppler perfusion imaging (LDPI). (**D**) Trichrome and H&E images of wound sections 31 days after treatment with different dermal substitutes showing quality of infiltrating tissue and residual cell response to scaffold remnants (high magnification, scale bars, 2 mm; low magnification, scale bars, 250 µm). (**E**) Semiquantitative analysis of wound healing through treatment-blinded pathohistological scoring of trichrome and H&E images for collagen deposition, epithelialization, and foreign body giant cells (FBGCs), yielding a cumulative wound healing score. Data are presented as means ± SEM (B and C) and means ± SD (E), $n = 6$ to 10 wounds, *$P < 0.05$, **$P < 0.01$, and ****$P < 0.0001$, by ANOVA.

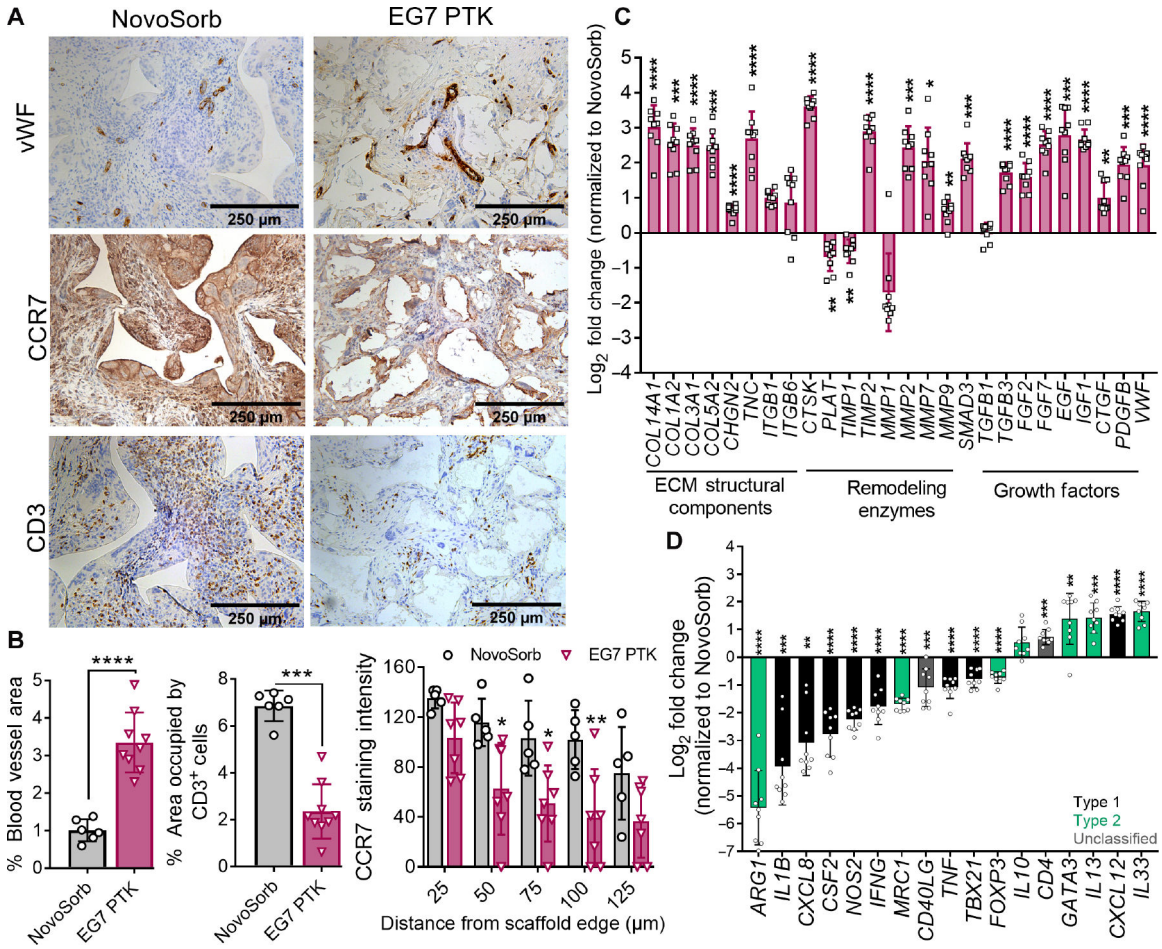

Fig. 7. EG7 PTK-UR scaffolds induce more vascularization and higher expression of wound healing–related and anti-inflammatory genes in day 31 pig wounds compared to NovoSorb.

(**A**) vWF, CCR7, and CD3 IHC images of NovoSorb- and EG7 PTK-UR–treated wounds. Scale bars, 250 μm. (**B**) Quantification of vWF-, CD3-, and CCR7-positive pixels using ImageJ. (**C**) Relative expression of genes encoding ECM components, remodeling enzymes, and growth factors related to wound healing and remodeling. (**D**) EG7 PTK-UR–treated wound expression of proinflammatory (black) and anti-inflammatory genes (green) (relative to NovoSorb). Data are presented as means ± SD, $n = 6$ to 10 wounds, $^{*}P < 0.05$, $^{**}P < 0.01$, $^{***}P < 0.001$, and $^{****}P < 0.0001$, by ANOVA.

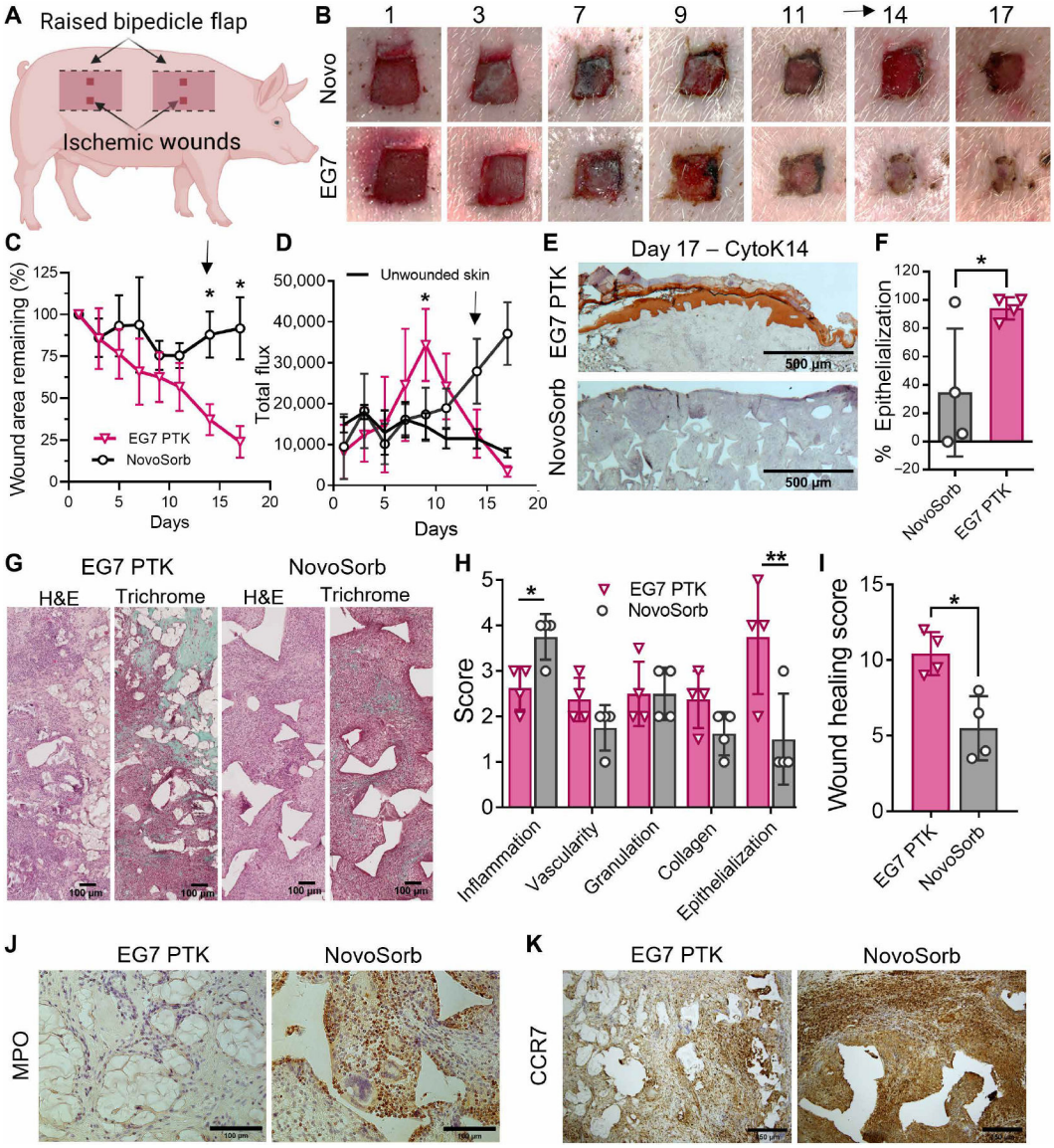

Fig. 8. EG7 PTK-UR scaffolds promote wound closure and reepithelialization of porcine ischemic wounds at day 17.

(**A**) Schematic of raised bipedicle ischemic flap model with excisional wounds. (**B**) Images over time of ischemic flap excisional skin wounds treated with NovoSorb or EG7 PTK-UR. (**C**) Kinetics of ischemic wound surface area change after treatment with PU foams. Arrow indicates time point of removal of NovoSorb protective upper layer. (**D**) Blood perfusion quantified as total flux within scaffold-implanted ischemic wound beds. Arrow indicates time point of removal of protective layer from NovoSorb, a procedure that disrupts granulation tissue and stimulates a neovascularization response. (**E** and **F**) Cytokeratin14 (CytK14) IHC visualization and quantification of end point percent wound reepithelization. (**G**) Representative microscopic images of wound sections stained with H&E and trichrome, showing the extent of cellular infiltration (pink/red in both images) and deposition of collagen (green in trichrome stain) within infiltrated voids of PU foams. (**H** and **I**) Wound healing subcategory scores and cumulative wound healing index. IHC showing spatial

organization and density of (**J**) MPO^+ neutrophils and (**K**) $CCR7^+$ macrophages. Data are represented as means ± SD, $n = 4$ wounds, $^*P < 0.05$ and $^{**}P < 0.01$, by ANOVA for (C) and (D) and *t* test for (F), (H), and (I). Arrows in (B) and (D) indicate the time of removal of the top layer of NovoSorb.